A Final Report

Entitled

Effect of Atmospherics on Beamforming Accuracy

Grant No. NAG 1-911

for the period
10/1/88 - 8/31/90

Submitted by

Texas A&M Research Foundation
College Station, Texas

to

National Aeronautics and Space Administration
Langley Research Center
Hampton, VA 23665-5225

Prepared by
Richard M. Alexander
Mechanical Engineering Department
Texas A&M University
College Station, TX 77843-3123

December 10, 1990

ABSTRACT

Two mathematical representations of noise due to atmospheric turbulence are presented. These representations are derived and used in computer simulations of the Bartlett Estimate implementation of *beamforming*. Beamforming is an array processing technique employing an array of acoustic sensors used to determine the bearing of an acoustic source. Atmospheric wind conditions introduce noise into the beamformer output. Consequently, the accuracy of the process is degraded and the bearing of the acoustic source is falsely indicated or impossible to determine. The two representations of noise presented here are intended to quantify the effects of mean wind passing over the array of sensors and to correct for these effects. The first noise model is an idealized case. The effect of the mean wind is incorporated as a change in the propagation velocity of the acoustic wave. This yields an effective phase shift applied to each term of the the spatial correlation matrix in the Bartlett Estimate. The resultant error caused by this model can be corrected in closed form in the beamforming algorithm. The second noise model acts to change the true direction of propagation at the beginning of the beamforming process. A closed form correction for this model is not available. Efforts to derive effective means to reduce the contributions of the noise have not been successful. In either case,

the maximum error introduced by the wind is a beam shift of approximately three degrees. That is, the bearing of the acoustic source is indicated at a point a few degrees from the true bearing location. These effects are not quite as pronounced as those seen in experimental results. Sidelobes are false indications of acoustic sources in the beamformer output away from the true bearing angle. The sidelobes that are observed in experimental results are not caused by these noise models. The effects of mean wind passing over the sensor array as modeled here do not alter the beamformer output as significantly as expected. More research is required to determine the cause of the sidelobe errors. Though smaller than expected, the effects of mean wind are quantified. If the wind may be represented by the first model, the effects of the wind may be eliminated. Correction for error caused by the second model is not currently possible.

TABLE OF CONTENTS

TABLE OF CONTENTS (Continued)

LIST OF FIGURES

LIST OF FIGURES (Continued)

LIST OF FIGURES (Continued)

LIST OF FIGURES (Continued)

LIST OF FIGURES (Continued)

Figure | Page

CHAPTER I

INTRODUCTION

Beamforming is a signal processing technique which uses an array of acoustic sensors to determine the bearing of an acoustic source. The outputs of the sensors are summed with weights and time delays to form a *beam*. The time delays are called *steering vectors* and their function is to sweep the beam through a range of assumed bearing angles. When the assumed direction corresponds to the true bearing angle, the magnitude of the beam is maximized. Beamforming is a passive detection technique. Data are digitally sampled from the outputs of acoustic sensors and then processed by computer. No energy is emitted as in active techniques such as radar.

Technology employing the acoustic principles on which beamforming is based was used as far back as World War I. These principles will be discussed in detail in Chapter II. Such processes were first developed by the British and the French to detect approaching bombers and zeppelins in the air and submarines in the ocean. However, these methods did not have sufficient accuracy to localize targets for aiming weapons. Towards the end of World War II, technology was developed to use radar for determining the range and bearing of enemy craft. Since World War II, most uses of passive detection techniques have been employed in water for the purpose of tracking. There are also geophysical applications for gathering information on seismic activity as discussed by Kleyn (1983). These applications are well documented and much research has been done in these areas.

Recently, interest has been renewed in the application of beamforming techniques to the tracking of acoustic sources (particularly helicopters) in the atmosphere. The advantage of beamforming is its passive nature. The acoustic sensor array emits no energy aimed at the target that the target can detect. This is not the case with the use of radar which emits a beam of electromagnetic energy and records echoes as the beam bounces off potential targets.

The accuracy of the beamforming process is degraded by noise in the signals from the acoustic sensors. The major portion of the noise is introduced as the acoustic waves pass through the medium. Variations in temperature and velocity of the air or water cause the path and speed of the acoustic waves to be varied. The result is increased uncertainty of the bearing angle of the target source. False indications may also be present. Due to the widespread use of beamforming applications in the ocean, the problem of noise in water has been addressed considerably and its characteristics are fairly well understood as discussed by Burdic (1984). The nature of noise due to atmospheric turbulence and how noise affects the beamforming process for the purpose of tracking in air has not received much attention. These topics are the subject of this report.

The *Bartlett Estimate* is the beamforming implementation discussed in this report. The Bartlett Estimate is but one beamforming algorithm. There are other high resolution techniques such as the *Maximum Likelihood Method* first reported by Capon (1969) and the *Linear Predictive Estimate* presented by Johnson (1982). These high resolution algorithms outperform the Bartlett Estimate in some cases. For example, these techniques are much better at distinguishing between two separate sources at close bearing angles where the Bartlett Estimate might identify the two as only being one source. A major drawback of such high resolution methods

is that a matrix inversion is required. In cases like tracking where averaging time is short, the matrices to be inverted may be singular and the methods fail. The Bartlett Estimate does not require matrix inversion and therefore can be applied to tracking.

Beamforming methods typically assume that noise is ideal. That is, the noise is assumed to be uncorrelated from sensor to sensor, spatially white and homogeneous. Therefore, the effects of the noise can theoretically be eliminated by long time averaging of the signal. Long time averaging is possible in cases where the source motion is small over the averaging time. However, in the case of a rapidly moving source or any case in which the averaging time is limited (e.g. tracking), the effects of noise are not negligible and cannot be averaged out. If a suitable representation of the noise due to atmospheric turbulence could be developed, it could then be used to modify the original data containing the acoustic signal and noise to yield a "cleaner" signal with which to carry out the beamforming process. Therefore, the accuracy of the beamformer would be enhanced. This report presents two such representations (models) for noise due to atmospheric turbulence. Computer simulations are performed to quantify the effects of noise having the form of these two models on the accuracy of the Bartlett Estimate beamformer. Both models require knowledge of the local wind conditions (speed and direction). The first model is idealized and a closed form solution is allowed. That is, the error induced by the wind can be eliminated within the beamforming algorithm. The second model is less idealized and a closed form solution is not available. Efforts to correct this error were unsuccessful.

THIS PAGE INTENTIONALLY BLANK

CHAPTER II

THE THEORY OF BEAMFORMING

The primary objective of beamforming is to determine the bearing of an acoustic source. An array of acoustic sensors is used to gather data on the acoustic energy in the air. The sensors record the acoustic vibrations in the air. These vibrations include contributions coming from the source at some unknown bearing angle and contributions from noise present in the atmosphere. The output of each sensor is multiplied by a weight a_i and given a time delay w_i. The adjusted outputs are then added to form the *beam*. Two assumptions are made:

1) The sound waves passing over the array are plane waves. This assumption provides that the source is sufficiently far away that the curvature of the acoustic wave is negligible over the sensor array.

2) The acoustic signal is only a function of time. No attenuation occurs over the distance traveled between sensors. The signal that each sensor receives is identical except for a phase shift (essentially a time delay) that arises from the different distances that the wave must travel from sensor to sensor.

Beamforming attempts to offset the phase shift (time delay) exactly at each sensor. When this is achieved, all the weighted sensor outputs are in phase and the magnitude of the beam is maximized. A beamformer is an example of a *spatial filter*. That is, acoustic energy arriving at bearing angles other than the true bearing angle are attenuated. The Bartlett Estimate studied in this thesis is presented by Nielsen (1989). The derivation of the Bartlett Estimate is presented next.

A target acoustic source is located at some unknown bearing angle θ. A unit

vector in the direction of the acoustic waves propagating from the acoustic source is $\hat{u}$. An array of M acoustic sensors is assembled and a coordinate system is defined. Each sensor has position vector $\bar{r}_i$ and a reference sensor is designated. See Figure 1. Note that the unit vector $-\hat{u}$ is located by the bearing angle θ. Let the reference sensor be sensor 1. The speed of sound in the air is c. The output at the ith sensor is given by

$$x_i(t) = s(t + \frac{\bar{r}_i \cdot \hat{u}}{c}) + n_i(t) \tag{2.1}$$

where s is the acoustic signal from the source and n is noise in the sensor output. The differential travel distance between sensor 1 and sensor i is $\bar{r}_i \cdot \hat{u}$ and is shown in Figure 2.

The time delay τ_i due to the differential travel distance is given by

$$\tau_i = \frac{\bar{r}_i \cdot \hat{u}}{c} \tag{2.2}$$

This is the time the plane wave takes to travel between sensor 1 to sensor i.

A bearing angle θ_0 is assumed and the unit vector pointing *from* this bearing direction is $\hat{u}_0$. The offsetting time delays τ_{i0} are then calculated as

$$\tau_{i0} = \frac{\bar{r}_i \cdot \hat{u}_0}{c} \tag{2.3}$$

The assumed bearing angle is swept through a range of assumed bearing directions.

The sensor outputs are given the offsetting time delays, multiplied by weights a_i and summed. This sum is called the "beam" or "beamformer." The beamformer output is denoted by $g(t)$ and is given by

$$g(t) = \sum_{i=1}^{M} a_i \Big[s(t + \frac{\bar{r}_i \cdot \hat{u}}{c} - \frac{\bar{r}_i \cdot \hat{u}_0}{c}) + n(t - \frac{\bar{r}_i \cdot \hat{u}_0}{c}) \Big] \tag{2.4}$$

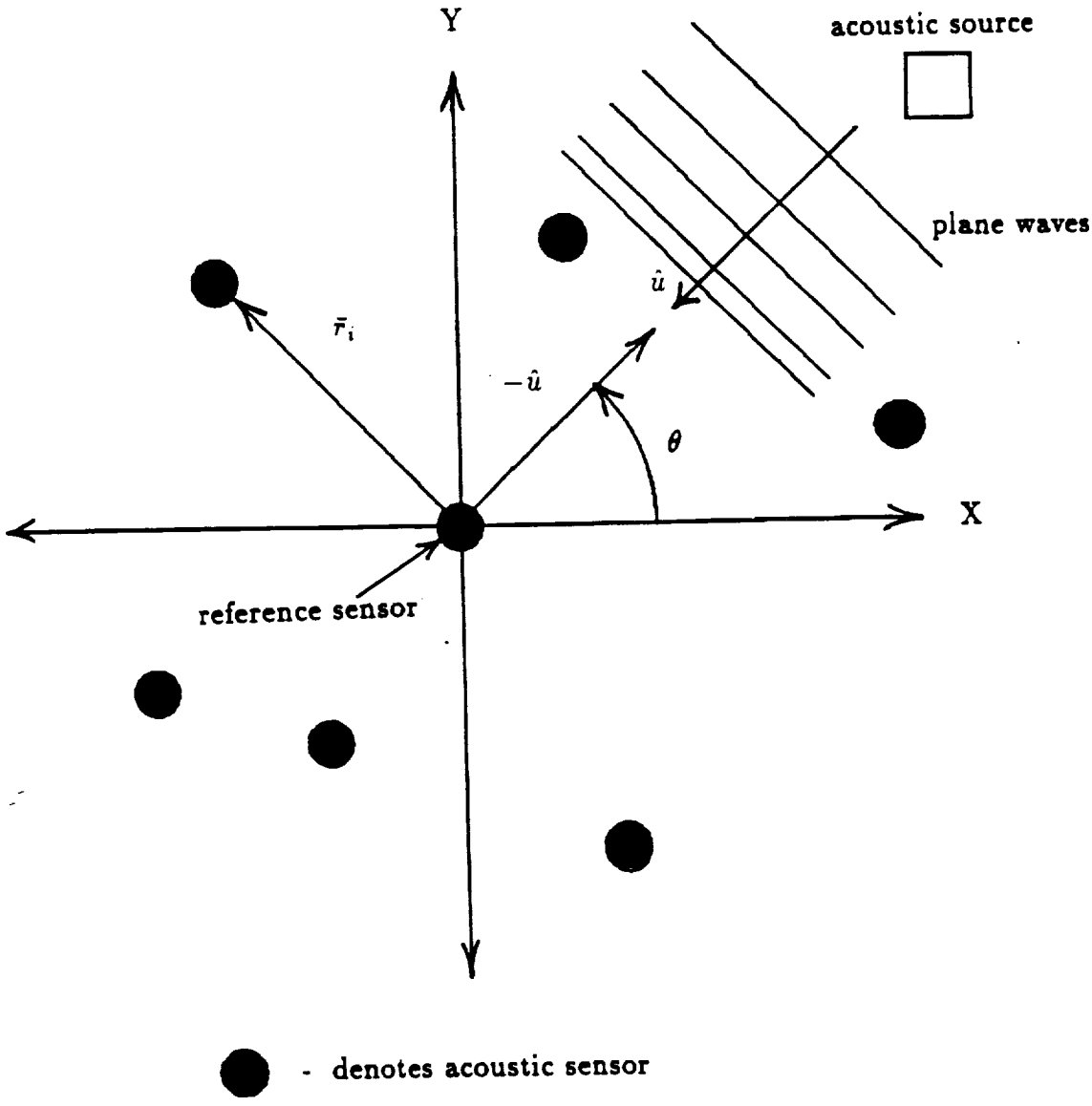

Figure 1. - General array of acoustic sensors.

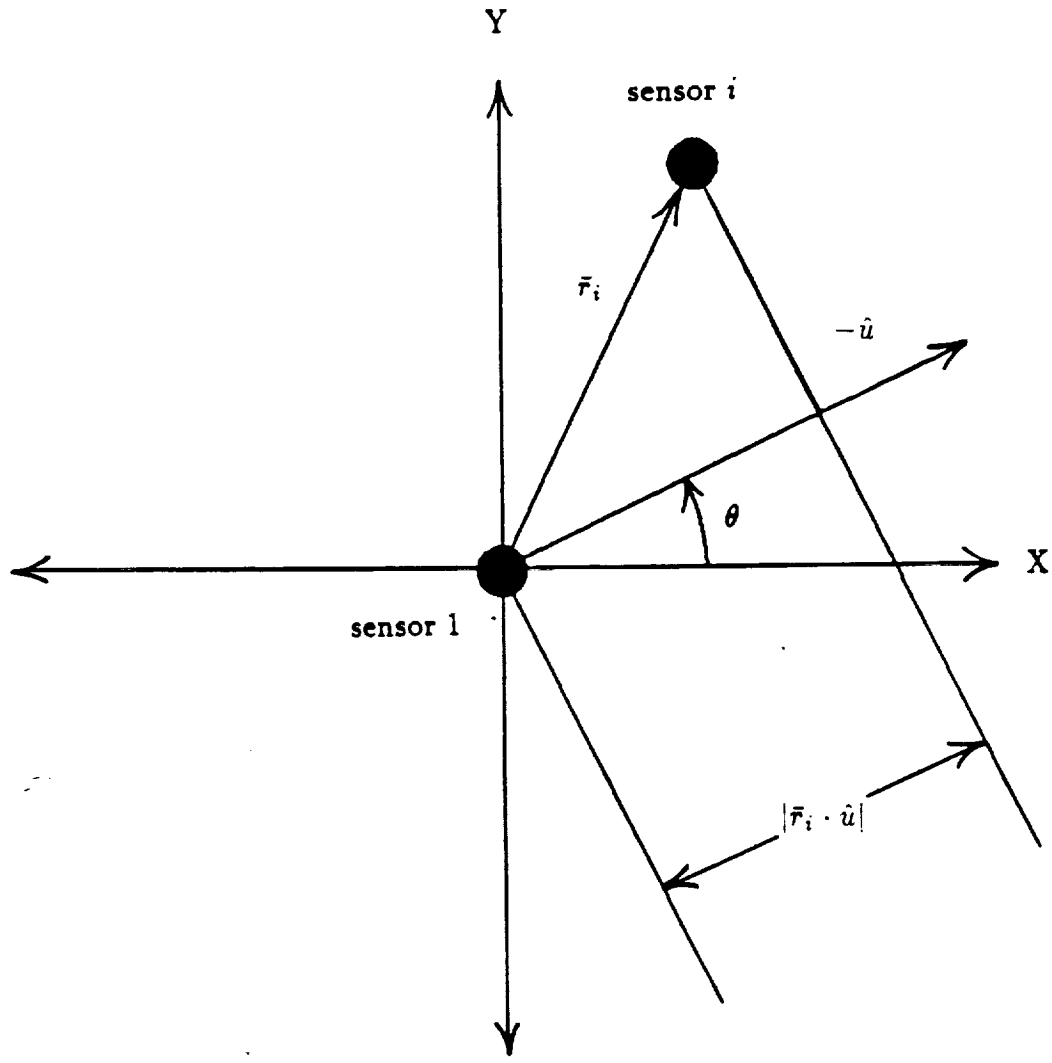

Figure 2. - Illustration of differential travel distance between sensor i and sensor 1.

When the assumed bearing angle corresponds to the true bearing angle, the offsetting time delays exactly cancel the delays of Equation 2.2, all of the sensor outputs are in phase and their sum is maximized. Assuming unity weights ($a_i = 1.0$) and letting τ_{i0} denote the offsetting time delays at each sensor as in Equation 2.3, the beamformer output is given as

$$g(t) = Ms(t) + \sum_{i=1}^{M} n(t - \tau_{i0}) \tag{2.5}$$

for the correct value of offsetting time delay τ_{i0}.

A. Frequency Domain Analysis

Further insight into the function of beamforming is gained by transforming these expressions into the frequency domain. The application of digital computers to beamforming in the frequency domain allows the use of fast algorithms such as the Fast Fourier Transform (FFT). Taking the Fourier Transform of Equation 2.4 yields the transform of the beamformer $G(f, \hat{u}_0)$. $G(f, \hat{u}_0)$ is a function of frequency, f, and assumed direction, $\hat{u}_0$, and is given by

$$G(f, \hat{u}_0) = \sum_{i=1}^{M} a_i X_i(f) \exp\left\{ \frac{-j2\pi f \bar{r}_i \cdot \hat{u}_0}{c} \right\} \tag{2.6}$$

where j is $\sqrt{-1}$ and $X_i(f)$ is the Fourier Transform of the sensor output

$$X_i(f) = S(f) \exp\left\{ \frac{j2\pi f \bar{r}_i \cdot \hat{u}}{c} \right\} + N_i(f) \tag{2.7}$$

Note that the offsetting time delays in Equation 2.4 are now represented by multiplication of complex exponentials which yield phase shifts in the frequency domain.

$G(f, \hat{u}_0)$ can be represented by a dot product of two vectors $\bar{w}$ and $\bar{x}$ which have components

$$\bar{w}_i = \exp\left\{\frac{-j2\pi f \bar{r}_i \cdot \hat{u}_0}{c}\right\} \quad \text{and} \quad \bar{x}_i = X_i(f)$$

The terms w_i are the steering vectors. Note that they include the assumed bearing angle θ_0. Then the beamformer is

$$G(f, \hat{u}_0) = \bar{w}^+ \cdot \bar{x} \tag{2.8}$$

where $^+$ denotes the complex conjugate transpose.

The power of the beam is a function of the square of the magnitude of the beam. With assumed direction $\hat{u}_0$ and at frequency f the power is given by

$$P(f, \hat{u}_0) = E\{|G(f, \hat{u}_0)|^2\} \tag{2.9a}$$

$$= \bar{w}^+ E\{\bar{x}\bar{x}^+\}\bar{w} \tag{2.9b}$$

$$= \bar{w}^+ \bar{R}\bar{w} \tag{2.9c}$$

where $E\{\bullet\}$ is the expectation operator which yields the average value of the argument. $\bar{R}$ is the *spatial correlation matrix.* The knth element of the spatial correlation matrix is given by

$$R_{kn} = E\{[S(f)\exp\{j2\pi f\frac{\bar{r}_k \cdot \hat{u}}{c}\} + N_k(f)]\times$$
$$[S^*(f)\exp\{-j2\pi f\frac{\bar{r}_n \cdot \hat{u}}{c}\} + N_n^*(f)]\} \tag{2.10}$$

where * denotes the complex conjugate. It is assumed that the signal and noise portions of the sensor outputs are completely uncorrelated (statistically independent). Therefore, the average of cross terms involving noise terms multiplied

by signal terms in Equation 2.10 are equal to zero. The spatial correlation matrix can then be expressed as

$$R_{kn} = E\left\{ S(f)S^*(f)\exp\{j2\pi f\frac{(\bar{r}_k - \bar{r}_n)\cdot\hat{u}}{c}\}\right\} + E\{N_k(f)N_n^*(f)\} \quad (2.11)$$

Defining the *spatial correlation matrix for noise* as

$$\bar{Q}_{kn} = \frac{E\{n_k(f)n_n^*(f)\}}{\sigma_n^2} \quad (2.12)$$

the beam output power is

$$P(f,\hat{u}_0) = \sigma_s^2\bar{w}^\top\exp\{j2\pi f\frac{(\bar{r}_k - \bar{r}_n)\cdot\hat{u}}{c}\}\bar{w} + \sigma_n^2\bar{w}^\top\bar{Q}\bar{w} \quad (2.13)$$

The expression in Equation 2.13 is the Bartlett Estimate for the power of the beamformer output. σ_s^2 and σ_n^2 are the intensities of the signal portion and the noise portion of the sensor outputs respectively. σ_s^2 is equal to $E\{S(f)S^*(f)\}$. The signal-to-noise ratio, SNR, is given by σ_s^2/σ_n^2. Note that $\bar{Q}$ is normalized by σ_n^2. The beamformer scans the range of assumed bearing angles for each frequency component in the range of frequencies of interest. In practice, much computer processing capability is required for the purpose of tracking since these ranges must all be covered in a time period that is approximately one second.

In Equation 2.13, σ_s^2, σ_n^2, $\hat{u}$ and $\bar{Q}$ are unknown quantities. The SNR in practice is usually small (on the order of 0 dB). The relative strengths of the signal and noise are important in determining the ability of a particular beamforming algorithm to pick out the signal when it is embedded noise. $\bar{Q}$ is the chief source of uncertainty because its composition is unknown. Many idealized models have been proposed to try to quantify the nature of $\bar{Q}$. The short averaging time characteristic to tracking causes poor performance of these models when applied to

the beamforming process. One such model is briefly discussed in the next chapter and three others are included in an appendix.

In experimental results, three primary effects on the beamformer performance are observed to be caused by atmospheric conditions. These effects are as follows:

1) Beam Shift - The indicated source bearing angle is displaced from the true bearing angle.

2) Beam Widening - The main peak in the beamformer output at the true bearing angle is widened. This adds uncertainty to the actual location of the maxima in beam power in practical implementation. The beam width is measured at the point where the beamformer power magnitude is 50% of the maximum beam power.

3) Presence of Sidelobes - Sidelobes are maxima in the beamformer power output at assumed bearing angles away from the true bearing angle. The sidelobes indicate that there are acoustic sources at other bearing angles when in fact there are none.

The matrix $\bar{Q}$ from Equation 2.13 contains the contribution of noise due to turbulence in the atmosphere. This quantity is unknown. If a suitable representation of $\bar{Q}$ could be determined, it could be subtracted from the right hand side of Equation 2.13 and a more accurate beamformer output would result.

CHAPTER III

APPLICATION OF BARTLETT ESTIMATE BEAMFORMER TO CURRENT WORK

A. Array Geometries and Spatial Aliasing

The range of frequencies over which a given geometry may be effectively used in beamforming is limited. The upper end of this range is limited by *spatial aliasing*. For a linear array with equally spaced sensors, the critical upper limit is the frequency whose wavelength λ is twice the sensor spacing d. When the frequency is greater than this critical value, the actual direction of propagation $\hat{u}$ may be confused with other assumed values of propagation $\hat{u}_0$. Aliasing causes considerable sidelobes thereby indicating sources where there are in fact none. The location(s) where spatial aliasing will cause false indications is uncertain. This is related to array geometry, the sensor spacing, d, the frequency, f, and the true bearing angle, θ. In practical applications, spatial aliasing is eliminated by low-pass

Figure 3.- Linear Sensor Array

filtering. It is important to know the critical frequency for the given array geometry. For the linear array with a sensor spacing of 1.8288 m (6 ft), the upper frequency limit is 94 Hz. Figure 4 gives an example of spatial aliasing. Beamformer outputs for $M = 10$, $d = 1.8288$ m (6 ft), $\theta = 45°$ and pure signal (no noise) are given for frequencies of 90 Hz and 140 Hz. The output for 140 Hz indicates a false source at 129°. Spatial aliasing is a phenomenon characteristic to beamforming and occurs given these conditions regardless of the noise model used or the array geometry. However, it can be minimized by array geometry. For example, inner sensors of the nested triangular array may be used to process higher frequencies than the outside sensors.

The lower range of frequencies is limited in that, as the frequency decreases, λ increases and becomes larger in comparison to the sensor spacing. The result is a broadening of the peak in beamformer output at the true angle of propagation and therefore the true angle of propagation becomes more uncertain. Figure 5 gives examples of this characteristic. Beamformer simulations for 30, 45, and 90 Hz with pure signal output for equal values of d, M and θ are shown. At 90 Hz, the half power point beam width is 15 degrees. At 45 Hz, it is 31 degrees. At 30 Hz, the half power point beam width is 54 degrees. The lower frequency limit should be set depending on the permissible beamwidth for a particular application. An upper limit recommended by Gerhold (1990) is the frequency whose wavelength $\lambda = 4d$.

Another consideration concerning the linear array configuration is symmetry. The output of a beamformer using a linear array is symmetric about the axis of the array line. That is, if the line connecting the sensors is the reference for zero degrees, any source, at 10° for example, will have an identical and yet *false* indication at $-10°$. This characteristic of the linear array is illustrated in Figure 6. In the

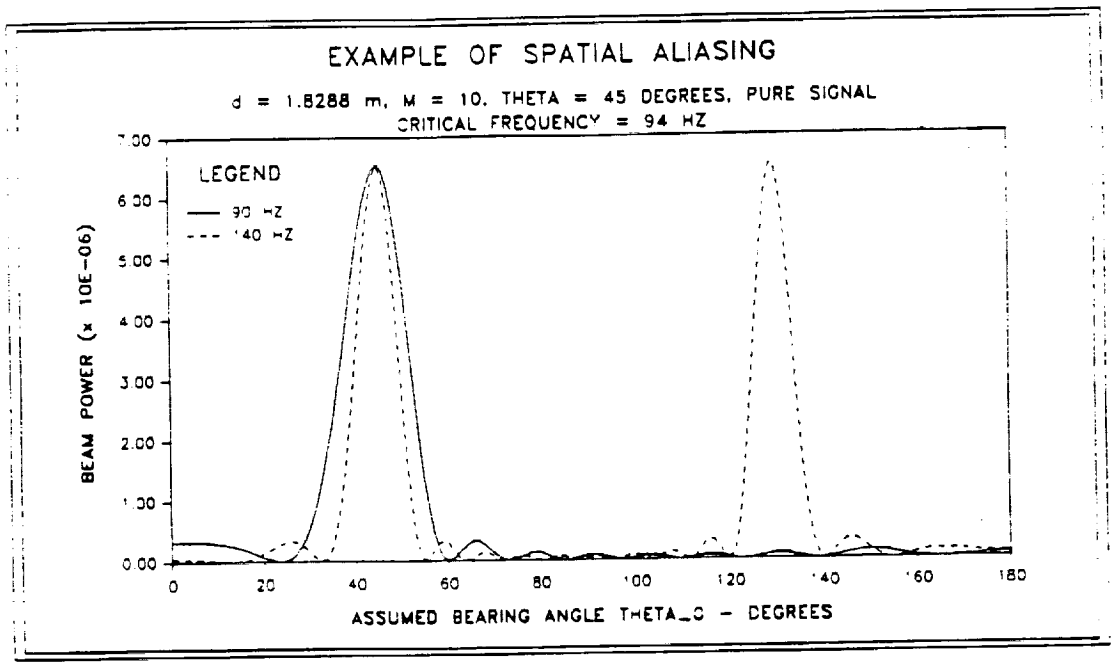

Figure 4. - Bartlett Estimate beamformer power output showing example of spatial aliasing. False indication is shown at 129°.

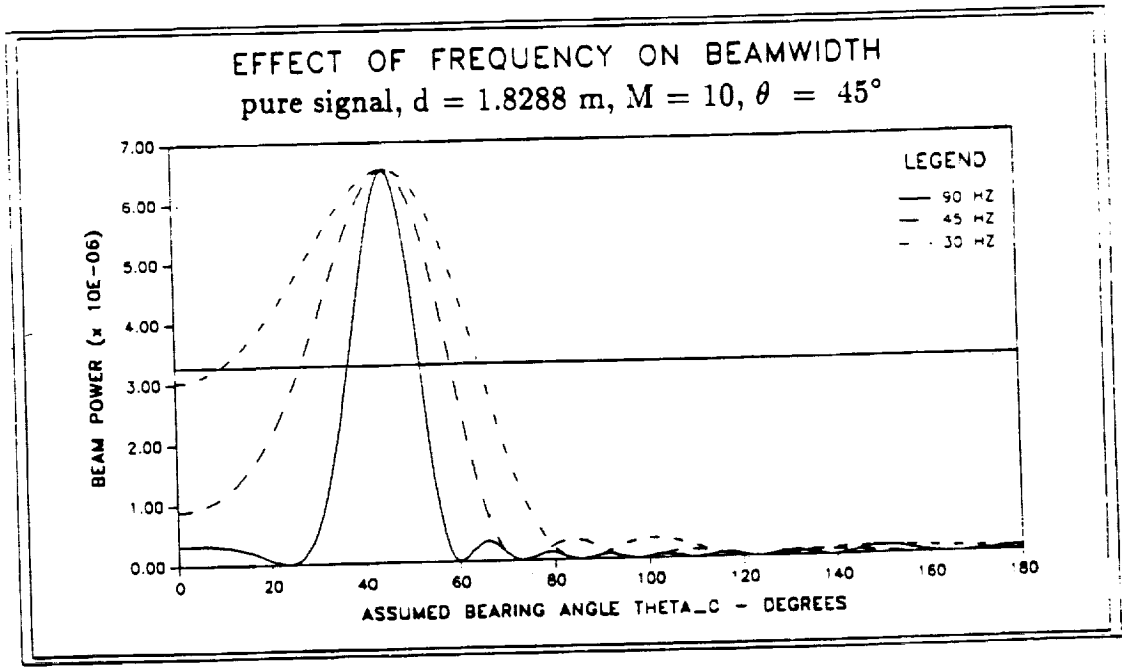

Figure 5. - Bartlett Estimate beamformer power output showing the effect of frequency, f, on the half power point beamwidth.

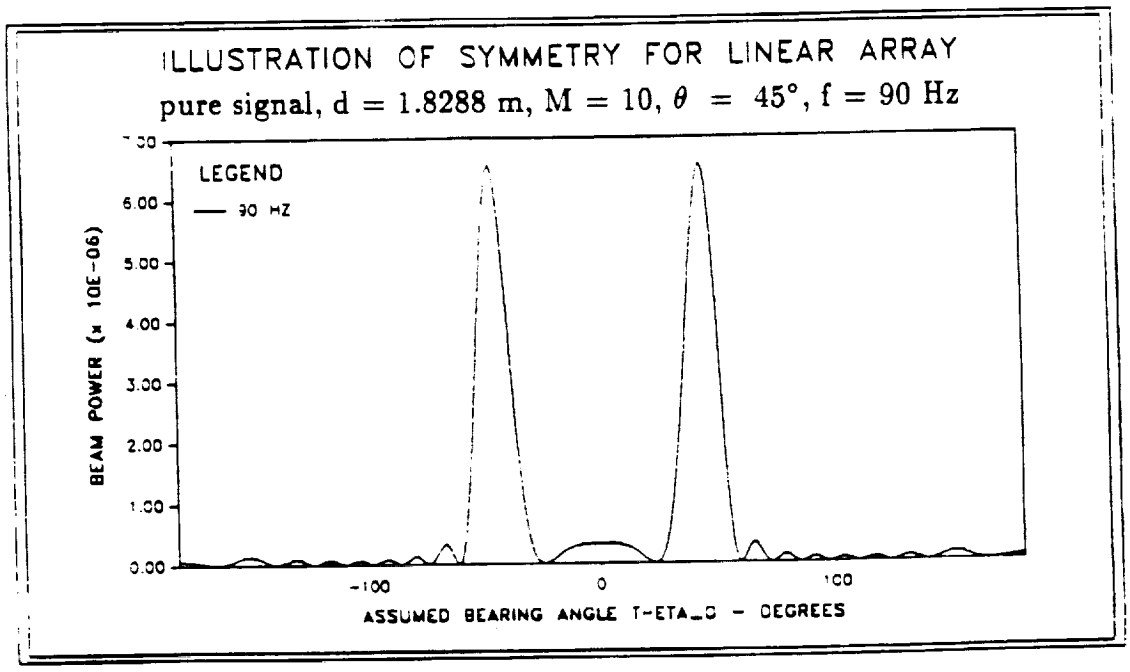

Figure 6. - Illustration of symmetry for the linear array of equally spaced acoustic sensors. True source is at 45°. False indication shown at −45°.

interest of space and clarity, most plots of beamformer output in this report will have 0° to 180° as a range for the assumed bearing angle θ_0.

B. Description of Beamformer Simulations

A linear array with equally spaced sensors as in Figure 3 was modeled. The sensor spacing d was 1.8288 m (6 ft). The half power point beam width is related to the number of sensors M. This is illustrated in Figure 7.

For identical values of d, f and θ, beamformer simulations were performed for values of M equal to 10, 15 and 20. For $M = 10$, the half power point beam width is 15 degrees. For $M = 15$, it is 10 degrees. For $M = 20$ it is 9 degrees. Note that as M is increased, the beam power increases as well. The number of sensors used here in the main simulations was $M = 10$. The speed of sound, c, used was 344 m/s (1128.0 ft/sec). This speed corresponds to a temperature of 294° K (70° F) at sea level. Discretized sine waves at a frequencies of 30, 45 and 90 Hz were generated and taken as the signal input to the sensors. (Recall that the frequency domain analysis of beamforming processes one frequency component at a time.) These frequency values yield results that are representative of beamformer output over the useful

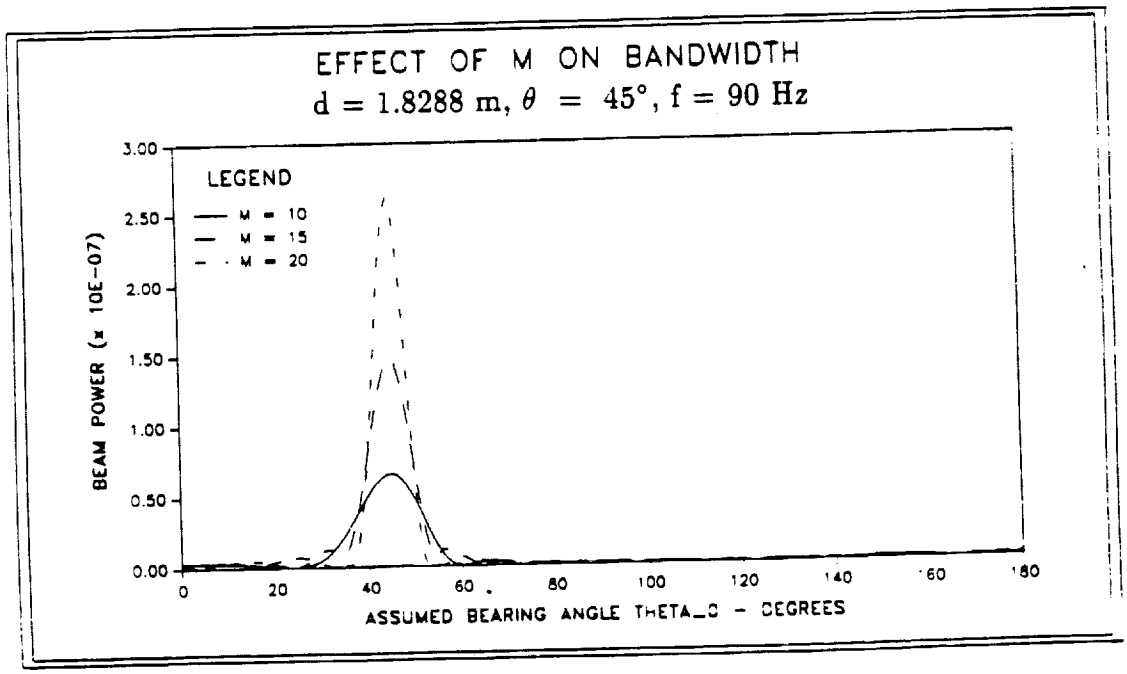

Figure 7. - Illustration of the effect of the number of sensors, M, on the half power point beamwidth of the Bartlett Estimate power output.

range of frequencies for the 1.8288 m (6 ft) sensor spacing. This useful range is the range of frequencies that the beamformer can be used to process. This useful range is limited on the high end by spatial aliasing. The low end is limited by beam widening. This range is related to the ratio of d/λ. Since the array geometries are typically fixed, the frequencies were varied while d was held constant to demonstrate beamformer behavior as the ratio d/λ changed. The upper aliasing limit where the wavelength $d = \lambda/2$ for $d = 1.8288$ m (6 ft) is 94 Hz.

It was assumed that the electronics introduce no noise into the sensor outputs. That is, the sensor outputs were modeled as pure, discrete sinusoids. A 512-point Fast Fourier Transform was taken of the signal outputs to transfer the data into the frequency domain.

All plots included to illustrate results present the magnitude of the beamformer power output on a linear scale. Typically, a decibel scale is used. However, a linear scale better shows the characteristics that are to be pointed out as results in this thesis.

Simulations were performed for different values of θ over the range of 0° to 180° for θ_0. Increments of one degree were taken. The frequency was 90 Hz. The beam width is dependent on the value of θ. As θ approaches the extremes of this range, the beam becomes wider. See Figure 8.

This beam widening is symmetric about 90°. For $\theta = 0^\circ$, the half power point beamwidth is 50 degrees. For $\theta = 30^\circ$ it is 23 degrees. For $\theta = 90^\circ$, it is 10 degrees. Recall that the beamformer output is symmetric about the line connecting the sensors in the linear array. This line is at zero degrees. As the beam moves toward zero degrees from the right, there is a corresponding beam moving toward zero from the left and these two begin to join together as they approach zero degrees

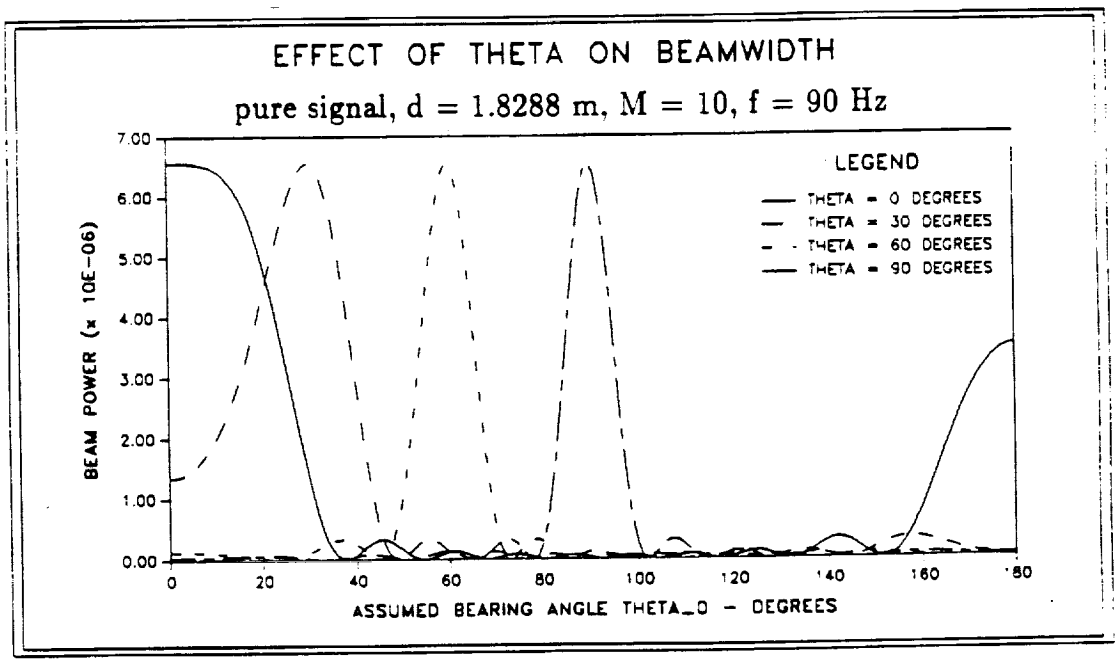

Figure 8. - Illustration of the effect of the true bearing angle, θ, on the half power point beamwidth of the Bartlett Estimate power output.

(or 180 degrees). This contributes to a very large half power point beam width near the extremes.

C. Criteria Used to Judge Performance of Noise Models

The power output of the Bartlett Estimate beamformer and the effects of the two proposed noise models on it are simulated in this report. Three criteria are used in judging the performance of the noise models in comparison to beamformer simulations with no noise included.

1) Shift in the location of the maximum beam power. This is the error in determining the "exact" true bearing angle of the acoustic source. See Figure 9 for an illustration of this shift.

2) Half power point beam width. This is the width in degrees of the peak in the beamformer output around the indicated true bearing angle corresponding to a power value of 50% of the peak power value. See Figure 10 for an illustration of the half power point beam width.

3) Presence of sidelobes. The presence of sidelobes indicate that a particular model causes false indications. That is, that the model would show that there are acoustic sources at bearing angles where there are in fact none. See Figure 11 for an example of sidelobes.

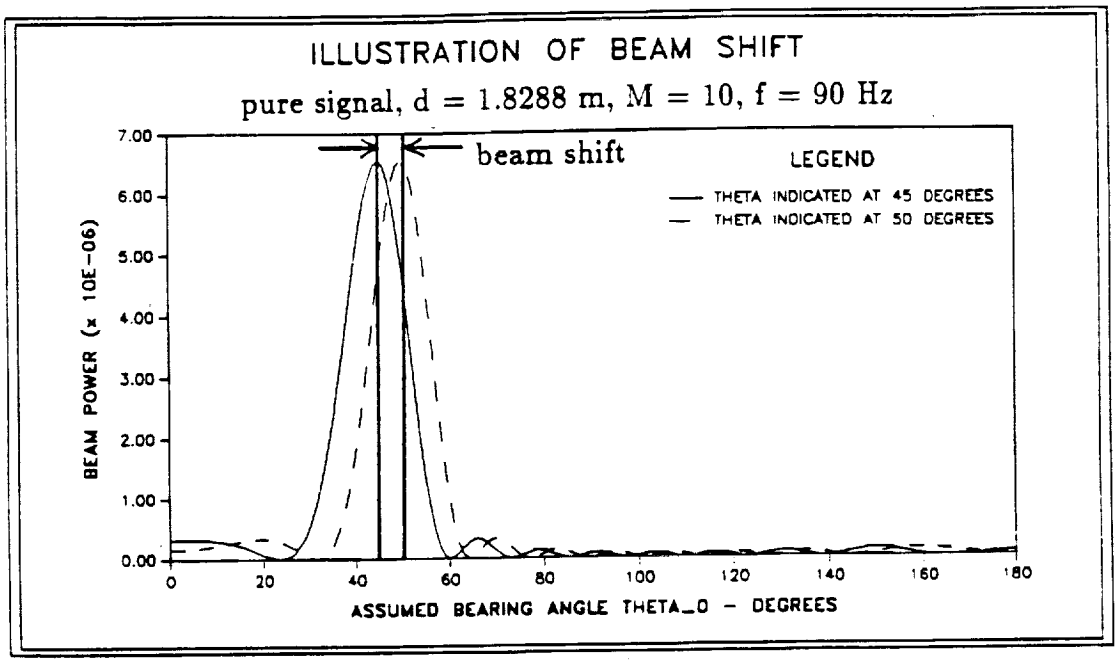

Figure 9. - Illustration of beam shift in the Bartlett Estimate beamformer power output. A beam shift of 5° is shown.

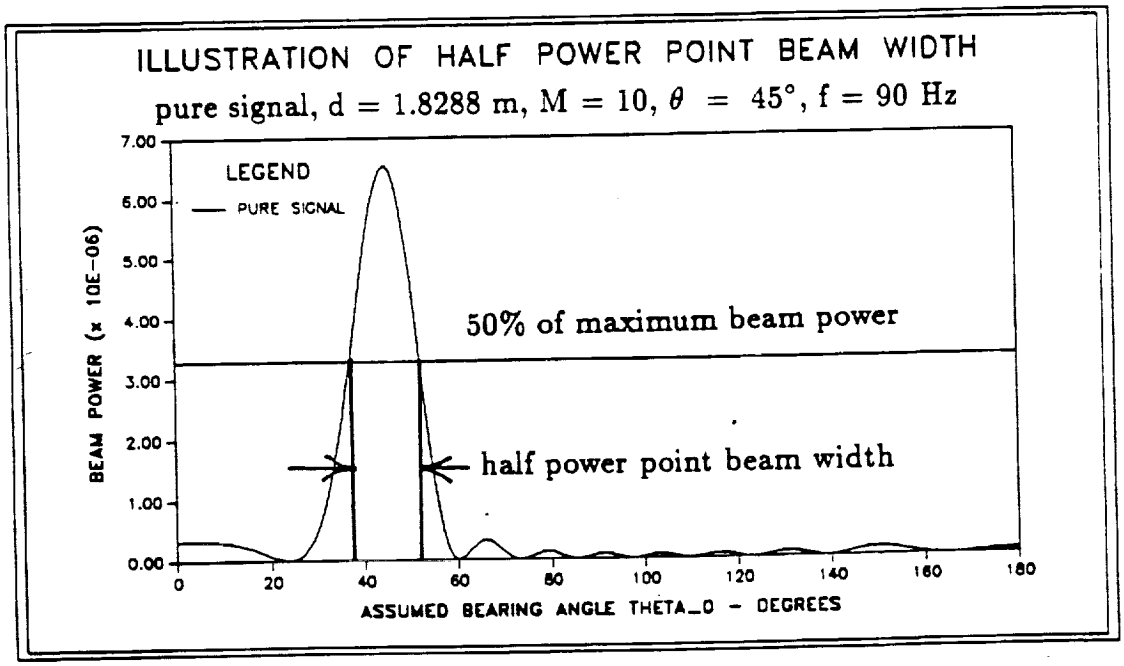

Figure 10. - Illustration of the beam width at the half power point of the Bartlett Estimate beamformer.

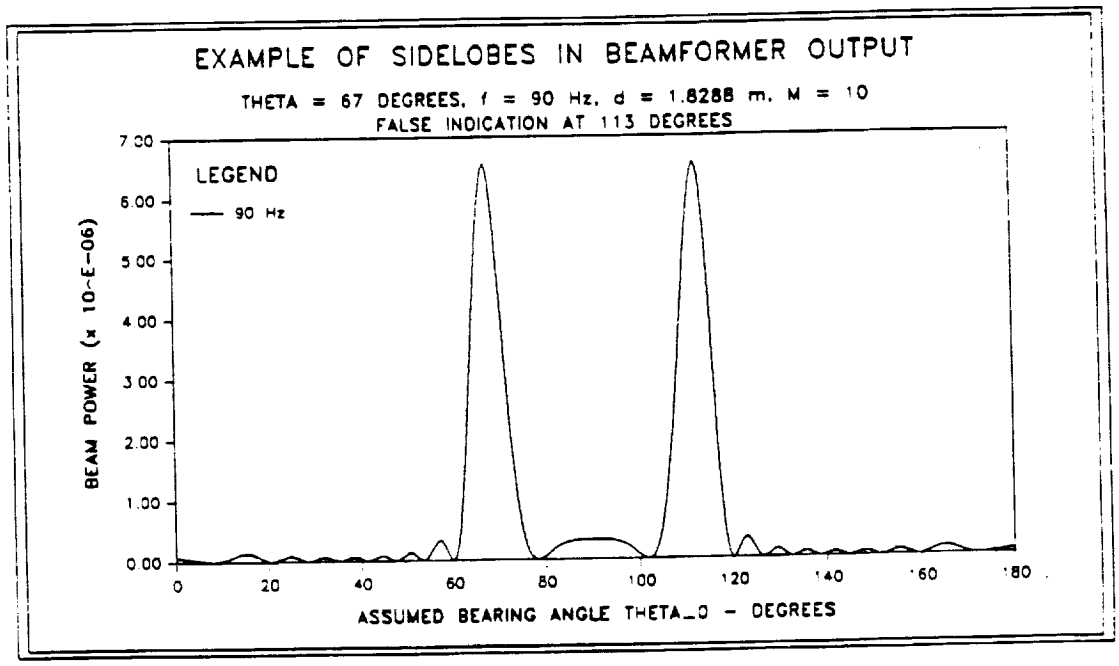

Figure 11. - Example of the presence of sidelobes in the Bartlett Estimate beamformer power output. The true bearing angle θ is 67°. A false indication of an acoustic source is present at 113° due to the sidelobe at that bearing angle.

CHAPTER IV

TWO REPRESENTATIONS OF NOISE DUE TO ATMOSPHERIC TURBULENCE

This chapter will present the two actual noise models proposed in the current work. The first is based on alteration of the speed of propagation and the second is based on shifting the direction of the propagation vector. The first is idealized and is correctable. The second is less idealized and efforts to correct it were unsuccessful.

A. Modification of Bartlett Estimate

A departure is taken from the Bartlett Estimate expression of Equation 2.13. The spatial correlation matrix for noise, $\bar{Q}$, is omitted and beam power is calculated from pure signal

$$P(f,\hat{u}_0) \;=\; \bar{w}^{+}\bar{R}_S\bar{w} \tag{4.1}$$

$\bar{R}_S$ is an *adjusted* spatial correlation matrix containing only signal information and no noise information. This is obtained from Equation 2.11. The knth element of $\bar{R}_S$ is given by

$$R_{S,kn} \;=\; S(f)S^{*}(f)\exp\{j2\pi f\frac{(\bar{r}_k \;-\; \bar{r}_n)\cdot\hat{u}}{c}\} \tag{4.2}$$

For the linear array, the dot product in Equation 4.2 is given by

$$(\bar{r}_k \;-\; \bar{r}_n)\cdot\hat{u} \;=\; (k \;-\; n)d\cos\theta \tag{4.3}$$

Rather than account for the presence of noise by using the matrix $\bar{Q}$, the noise is represented by an alteration of the phase shift information of $\bar{R}_S$. How this is accomplished for each of the two noise models will be discussed in detail later in

this chapter. A wind speed of 13.4 m/s (44 ft/sec) was used. On flat land, this is a realistic order of magnitude mean wind velocity for a short sustained gust as presented by Stull (1988) and recommended by North (1990).

Each case of modeling the noise due to atmospheric turbulence is compared to the calculation of beam power with no noise as given by Equation 4.1. This allows the full effect of the wind to be isolated and observed.

B. Noise Model 1

The first noise model assumes that the wind alters the speed of propagation of the acoustic waves. The direction of the propagation vector is assumed to be unaffected. Doppler effects are also ignored. The projection of the wind velocity onto the vector of the true propagation velocity adds to the speed of sound c and effectively changes the speed at which the plane wave travels through the atmosphere. The change in velocity alters the time delay which occurs as the wave passes from one sensor to another. Recall from Equation 2.2 that the time delay is dependent on the propagation velocity. Since the beamformer attempts to negate these phase shifts based on the propagation speed in still air, an error will be introduced. This error will result when the phase shifts represented in $\bar{R}_S$ and in the steering vectors $\bar{w}_i$ will be equivalent but the assumed angle of propagation and the true angle of propagation will not be the same.

Recall the definition of the knth element of the spatial correlation matrix for pure signal $\bar{R}_S$

$$R_{S,kn} = S(f)S^*(f)\exp\{j2\pi f\frac{(\bar{r}_k - \bar{r}_n)\cdot\hat{u}}{c}\} \tag{4.4}$$

A unit vector pointing from the true bearing direction is $\hat{u}$. The true bearing of the acoustic source is θ. Now consider a wind blowing at constant velocity V in the direction defined by a unit vector $\hat{p}$. The bearing angle of the direction that the wind is coming from is θ_W. See Figure 12. Unit vector $-\hat{p}$ points in this direction. The wind acts to change the phase shift between two given sensors.

Consider the time delays between the kth and nth sensors. The extra distance that the plane wave must travel after passing sensor n before sensor k receives it is ρ_{kn} given by

$$\rho_{kn} = (n - k)d\cos\theta \tag{4.5}$$

This distance is illustrated in Figure 13. The speed of sound in still air is c and then the corresponding time delay τ_{kn} is ρ_{kn}/c.

$$\tau_{kn} = \frac{(n - k)d\cos\theta}{c} \tag{4.6}$$

Now let the wind velocity component along $\hat{u}$ be added to c. The adjusted speed of propagation is given by

$$c + V\cos(\theta_W - \theta)$$

Figure 14 illustrates the vector operations that yield this result.

The adjusted time delay which occurs now between the nth and kth sensors is $\tau_{a,kn}$ and is given by

$$\tau_{a,kn} = \frac{(n - k)d\cos\theta}{c + V\cos(\theta_W - \theta)} \tag{4.7}$$

The difference between time delays without wind and with wind (the difference between Equation 4.6 and Equation 4.7) is $\tau_{d,nk}$ and is given by

$$\tau_{d,kn} = (n - k)d\cos\theta\left(\frac{1}{c} - \frac{1}{c + V\cos(\theta_W - \theta)}\right) \tag{4.8}$$

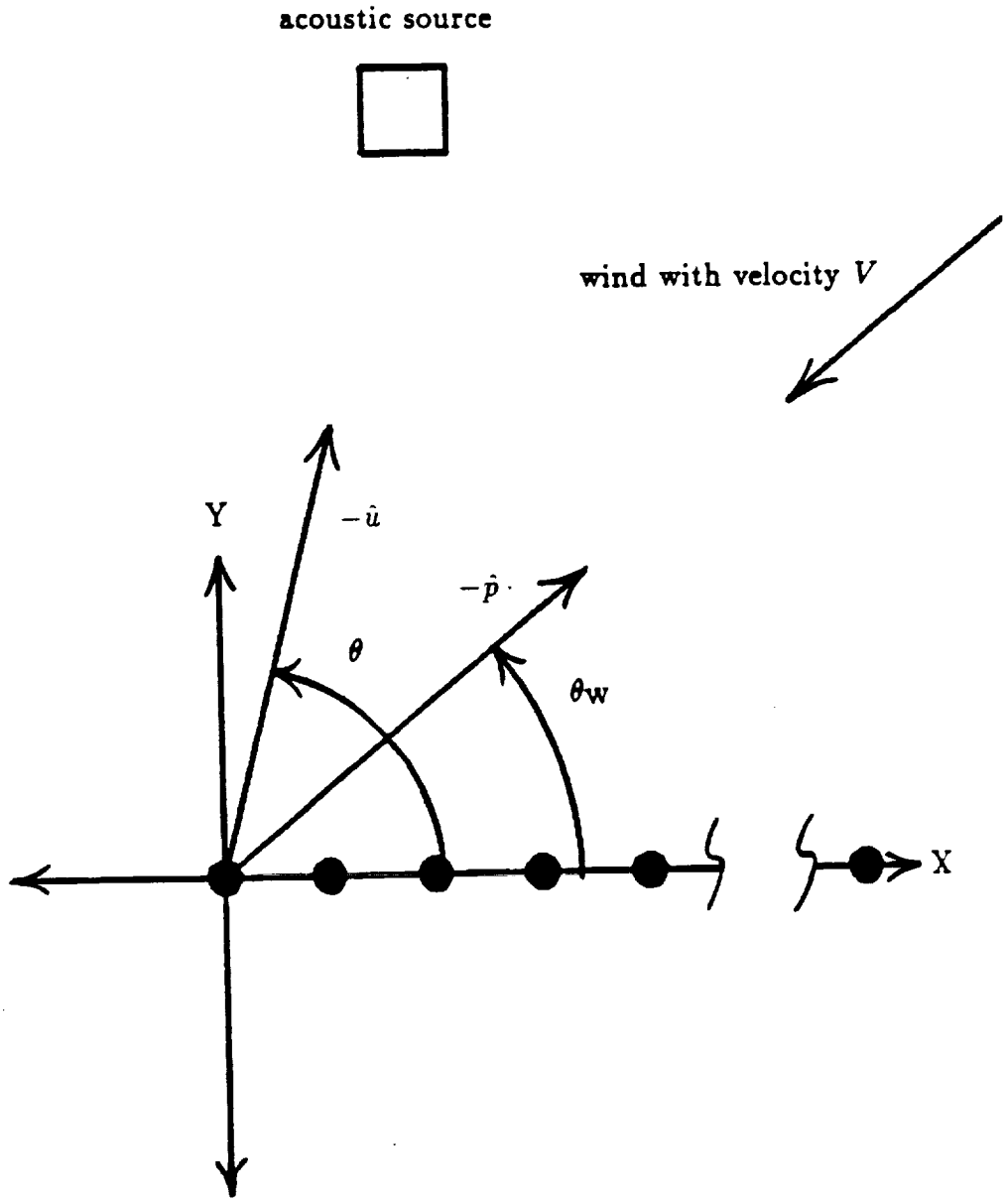

Figure 12. - Mean wind at velocity V coming from bearing angle θ_W blowing over a linear sensor array.

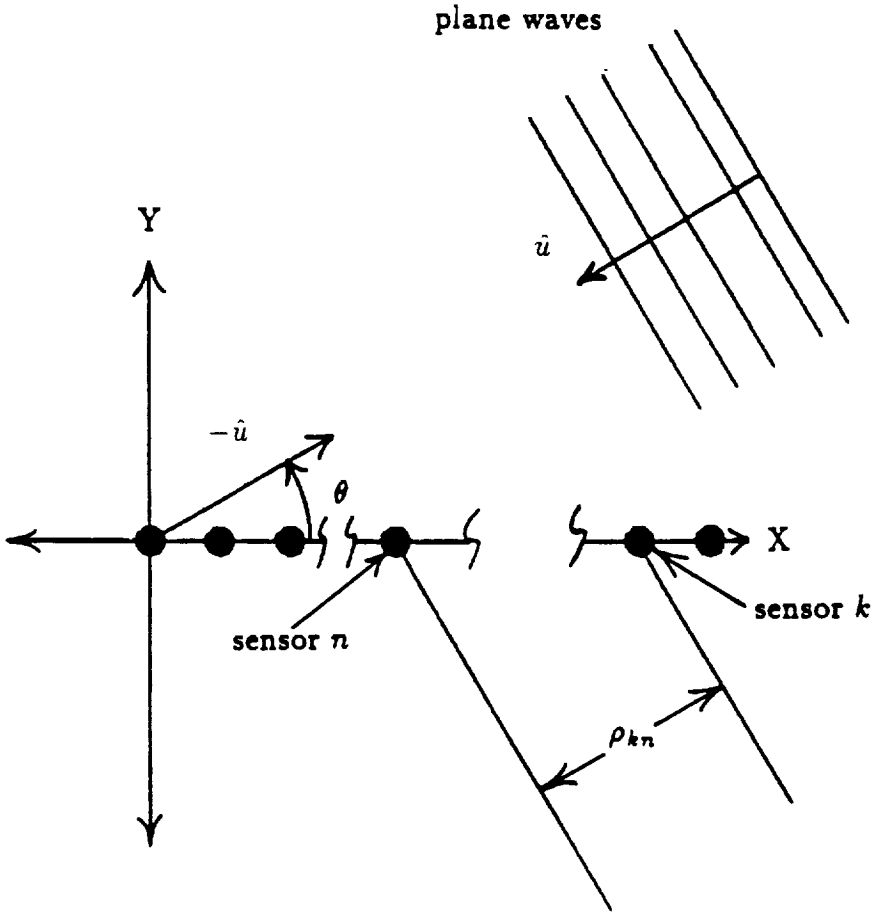

Figure 13. - Illustration of the differential travel distance between the kth and nth sensors of a linear array with sensor spacing d.

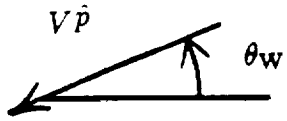

(a)

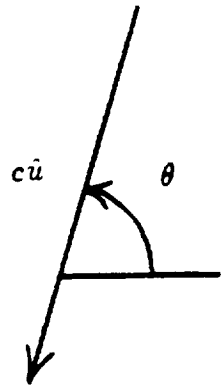

(b)

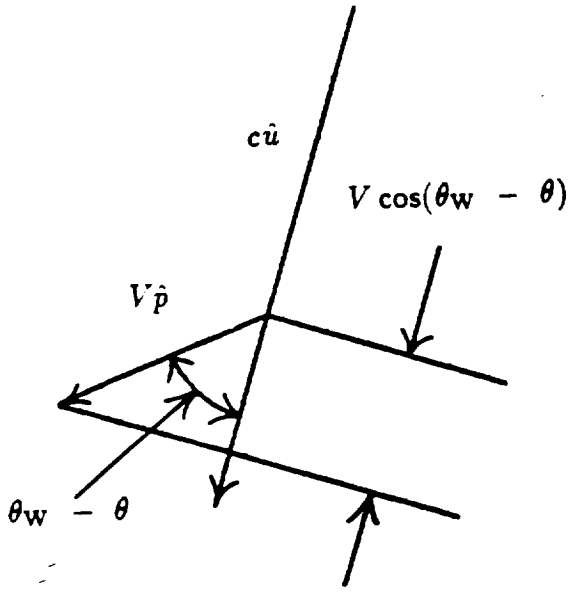

(c)

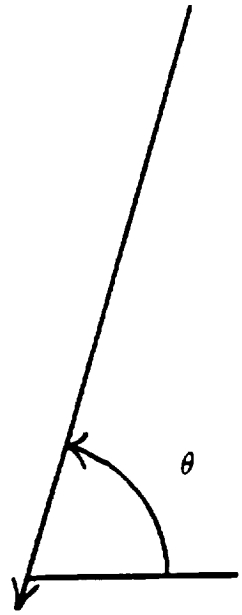

$[c + V\cos(\theta_W - \theta)]\hat{u}$

(d)

Figure 14. - Vector additions of wind and sound propagation vectors for Noise Model 1. (a) Wind vector. (b) Sound propagation vector in still air. (c) Projection of the wind vector in the direction of propagation vector shown in (b). (d) Resultant adjusted propagation vector with unaffected direction but with adjusted magnitude.

In the frequency domain, this time delay corresponds to a phase shift ϕ which, in radians, is $2\pi f \tau_{d,kn}$. A phase shift is represented by a complex multiplication in the frequency domain. This phase shift can be used to alter the phase characteristics of the matrix $\bar{R}_S$ by multiplying the knth element of $\bar{R}_S$ by $e^{j\phi_{kn}}$. This defines the spatial correlation matrix for the first model, $\bar{R}_1$. This phase shift is given by

$$\phi_{kn} = 2\pi f(n - k)d\cos\theta\left(\frac{1}{c} - \frac{1}{c + V\cos(\theta_W - \theta)}\right) \tag{4.9}$$

The knth element of $\bar{R}_1$ is given by

$$\bar{R}_{1,kn} = \bar{R}_{S,kn}e^{j\varphi_{kn}} \tag{4.10}$$

Then the beam power taking into account the effect of mean wind as prescribed by this model is

$$P(f,\hat{u}_0) = \bar{w}^+\bar{R}_1\bar{w} \tag{4.11}$$

Equation 4.9 shows that the maximum *magnitude* of error introduced by this model would occur when the source was at an angle of 0° or 180° and the quantity $(\theta_W - \theta)$ was equal to π. The direction of beam shift would depend on whether θ was 0 or 180 degrees. That is, the phase shift angle ϕ_{kn} from Equation 4.9 is maximized for this set of conditions. The greatest change applied to the the velocity c occurs then since the $\cos\theta$ factor is equal to ± 1 and the factor $1/[c + V\cos(\theta_W - \theta)]$ is maximized at $1/(c - V)$. Note that the $\cos\theta$ factor scales down the effect as θ approaches $\pm\pi/2$ from either side. When θ equals $\pm\pi/2$, ϕ_{kn} equals zero and there is no effect at all regardless of the magnitude of V because the $\cos\theta$ factor drives the whole term to zero. This is so because the plane waves are reaching all of the sensors at the same time (broadside). Also, there is no effect when $\hat{u}$ and $\hat{p}$ are orthogonal because in this case, the projection of the wind velocity in the direction

of $\hat{u}$, $\cos(\theta_W - \theta)$, becomes zero. Figures 15 through 20 show representative beamformer outputs for frequencies of 30, 45 and 90 Hz with θ equal to 30° and 60°. The mean wind velocity V used was 13.4 m/s (44 ft/sec) and θ_W was set equal to θ for each case.

C. Correction of Error Caused by Noise Model 1

The effect of noise of the form of that proposed by Model 1 may be corrected. Since this effect is essentially a phase shift applied to the matrix $\bar{R}_S$, (given in Equation 4.10), the matrix $\bar{R}_1$ may be multiplied by another phase shift, synthesized from available wind data, that negates the phase shift caused by the wind. Note that $e^{\phi}e^{-\phi} = 1$.

Equation 4.9 defines the phase shift ϕ_{kn} applied to the knth element of the matrix $\bar{R}_S$. If the respective elements of $\bar{R}_1$ could be multiplied by a term $e^{-j\phi_{kn}}$, then the effects of the mean wind would be completely eliminated. The exact values of ϕ_{kn} are not known however because Equation 4.9 requires knowledge of the true bearing angle θ. This is the quantity that is sought. Instead, the assumed bearing angle θ_0 is used in place of θ to give the correction phase shift γ.

$$\gamma_{kn} = 2\pi f(n - k)d\cos\theta_0\left(\frac{1}{c} - \frac{1}{c + V\cos(\theta_W - \theta_0)}\right) \tag{4.12}$$

The knth element of the corrected spatial correlation matrix for the first noise model $\bar{R}_{1C}$ is given by

$$\bar{R}_{1C,kn} = \bar{R}_{1,kn}e^{-j\gamma_{kn}} \tag{4.13}$$

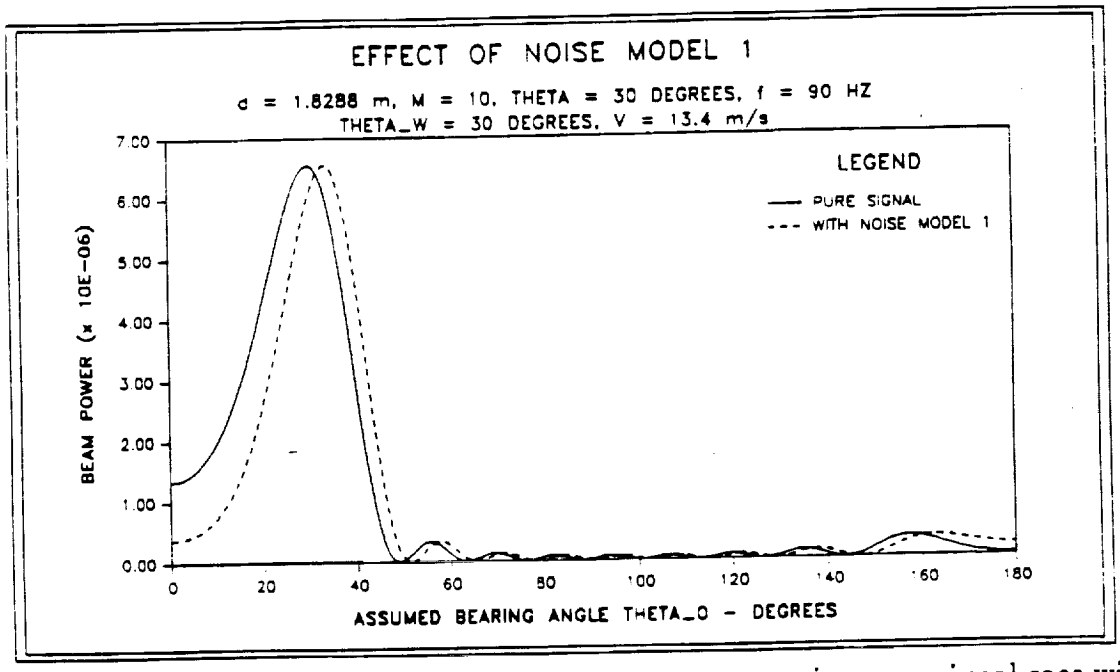

Figure 15. - Bartlett Estimate beamformer output comparing pure signal case with output including atmospheric effects modeled by Noise Model 1 for $f = 90$ Hz and $\theta = 30°$.

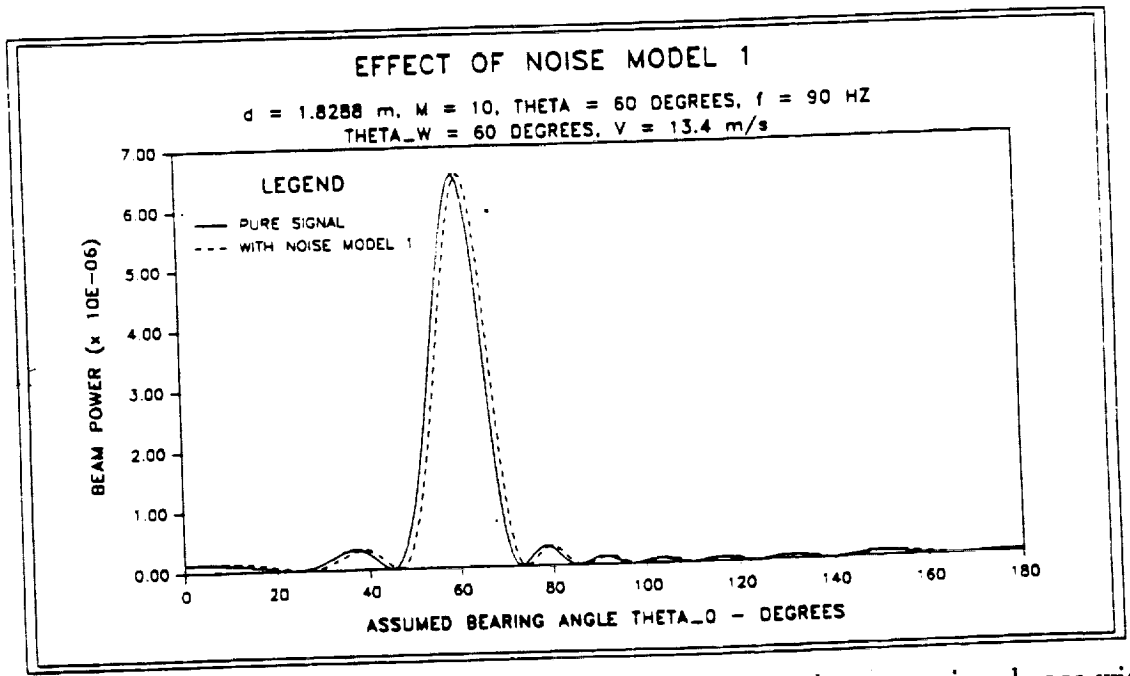

Figure 16. - Bartlett Estimate beamformer output comparing pure signal case with output including atmospheric effects modeled by Noise Model 1 for $f = 90$ Hz and $\theta = 60°$.

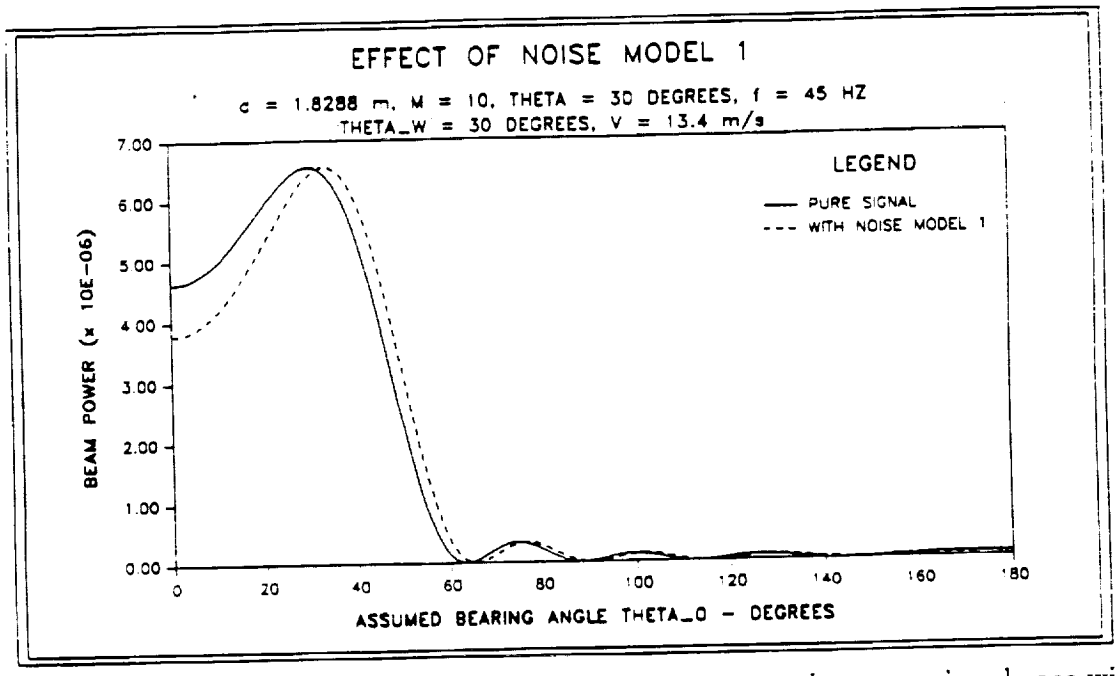

Figure 17. - Bartlett Estimate beamformer output comparing pure signal case with output including atmospheric effects modeled by Noise Model 1 for $f = 45$ Hz and $\theta = 30°$.

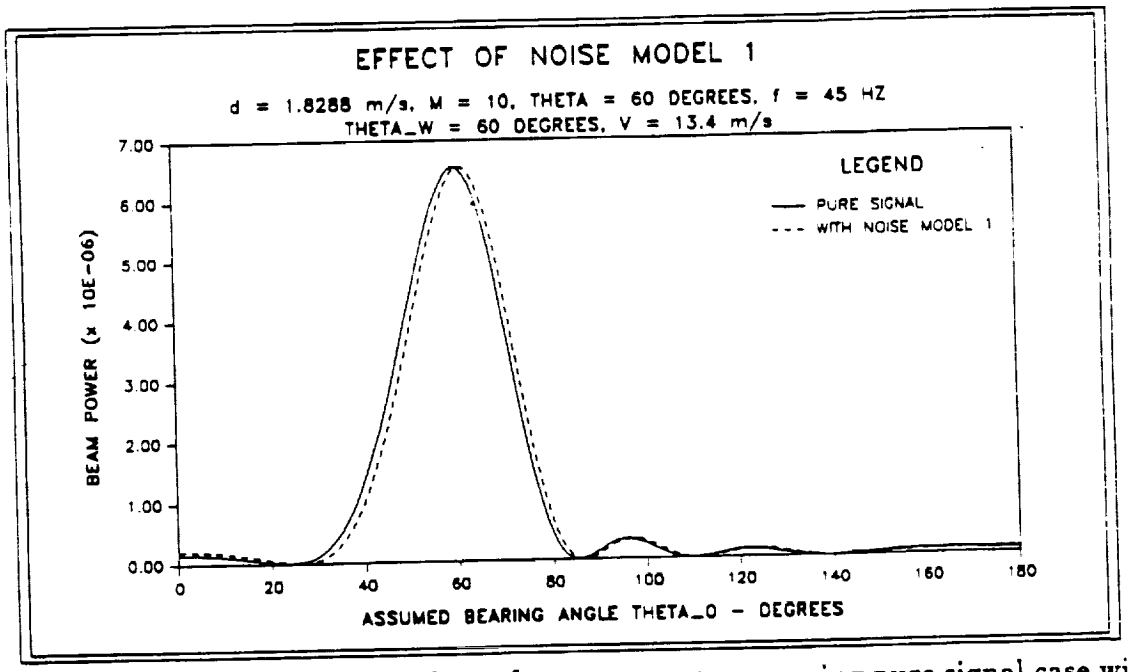

Figure 18. - Bartlett Estimate beamformer output comparing pure signal case with output including atmospheric effects modeled by Noise Model 1 for $f = 45$ Hz and $\theta = 60°$.

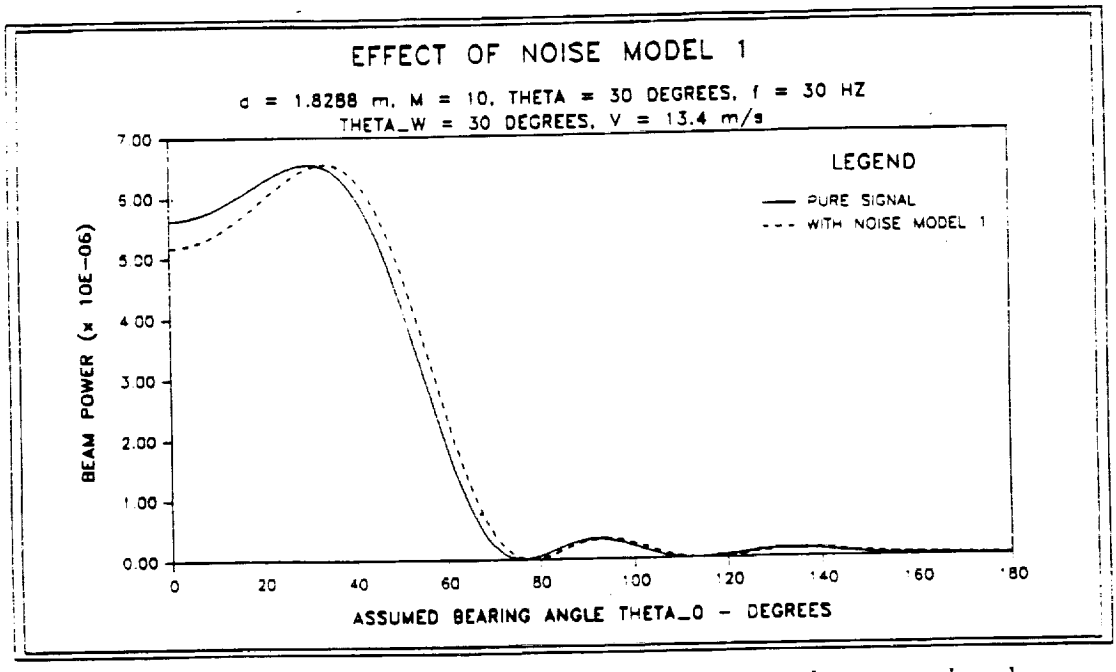

Figure 19. - Bartlett Estimate beamformer output comparing pure signal case with output including atmospheric effects modeled by Noise Model 1 for $f = 30$ Hz and $\theta = 30°$.

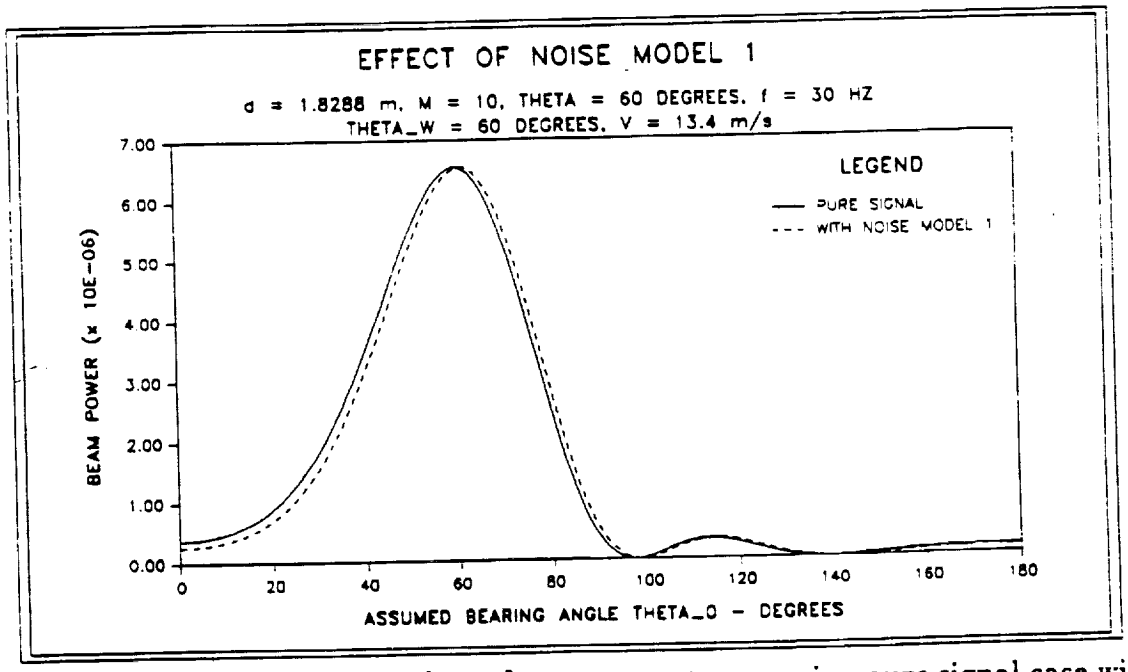

Figure 20. - Bartlett Estimate beamformer output comparing pure signal case with output including atmospheric effects modeled by Noise Model 1 for $f = 30$ Hz and $\theta = 60°$.

The beam power for the correction is then given by

$$P(f, \hat{u}_0) = \bar{w}^+ \bar{R}_{1C} \bar{w} \tag{4.14}$$

At values of θ_0 near θ, the correction is virtually exact. See Figures 21 through 26 for representative results of these beamformer simulations for frequencies of 30, 45 and 90 Hz and for values of θ equal to 30° and 60°. The mean wind velocity was 13.4 m/s (44 ft/sec) and θ_W was set equal to θ for each case. As these figures show, the beam shift caused by mean wind as represented by Model 1 can be totally eliminated.

D. Noise Model 2

The first proposed noise model assumed that the wind only affected the speed of propagation of the acoustic waves and not the direction. The second model to be shown now assumes that the wind only affects the direction of propagation and not the speed. As with the previous model, consider a wind at constant velocity V blowing over the array with bearing angle θ_W. Refer back to Figure 12. Let the wind vector and the true propagation vector add together to form a new propagation vector $\bar{U}_2$. The resultant x component is given by

$$U_{2x} = -c \cos\theta - V \cos\theta_W \tag{4.15}$$

and the resultant y component is given by

$$U_{2y} = -c \sin\theta - V \sin\theta_W \tag{4.16}$$

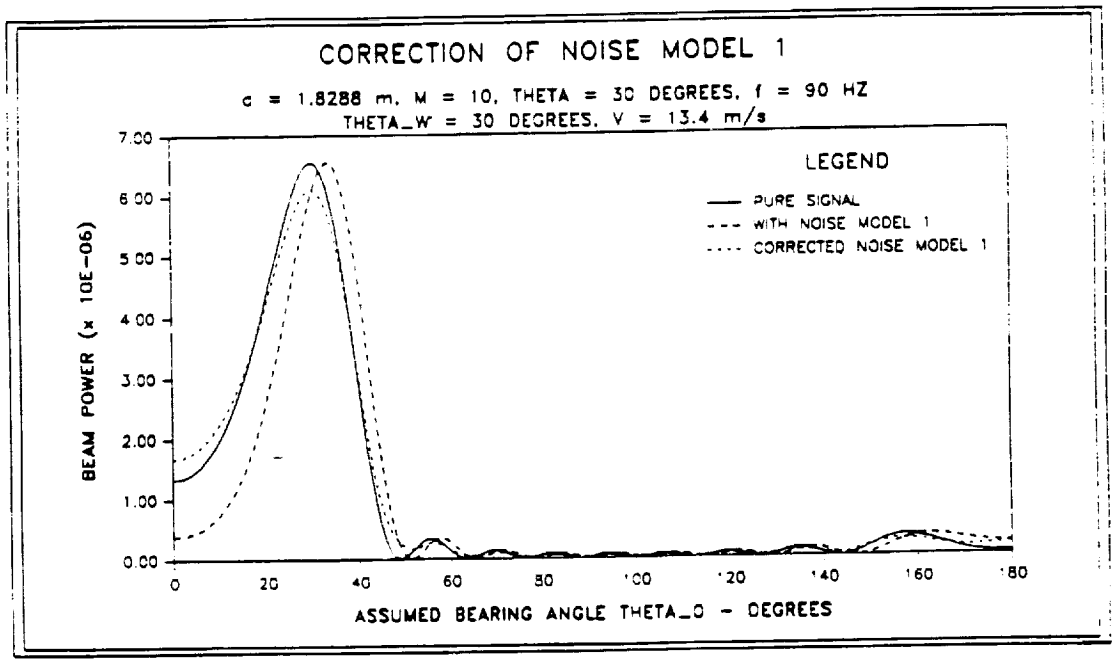

Figure 21. - Bartlett Estimate beamformer output comparing pure signal case with output including atmospheric effects modeled by Noise Model 1 and the case of the corrected Noise Model 1 for $f = 90$ Hz and $\theta = 30°$.

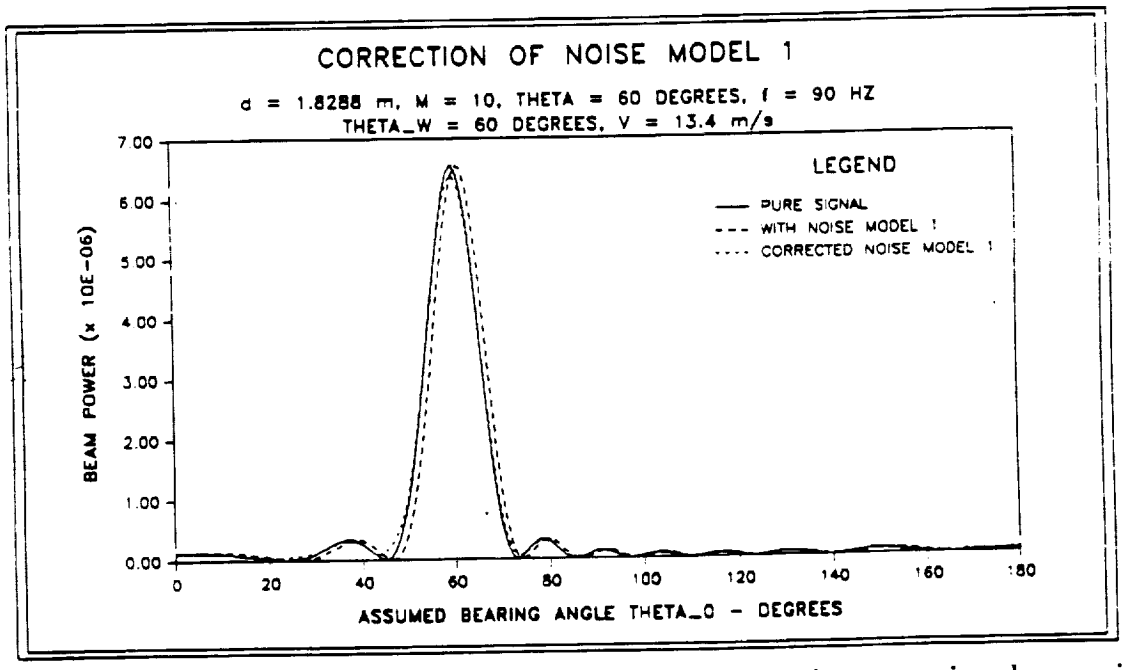

Figure 22. - Bartlett Estimate beamformer output comparing pure signal case with output including atmospheric effects modeled by Noise Model 1 and the case of the corrected Noise Model 1 for $f = 90$ Hz and $\theta = 60°$.

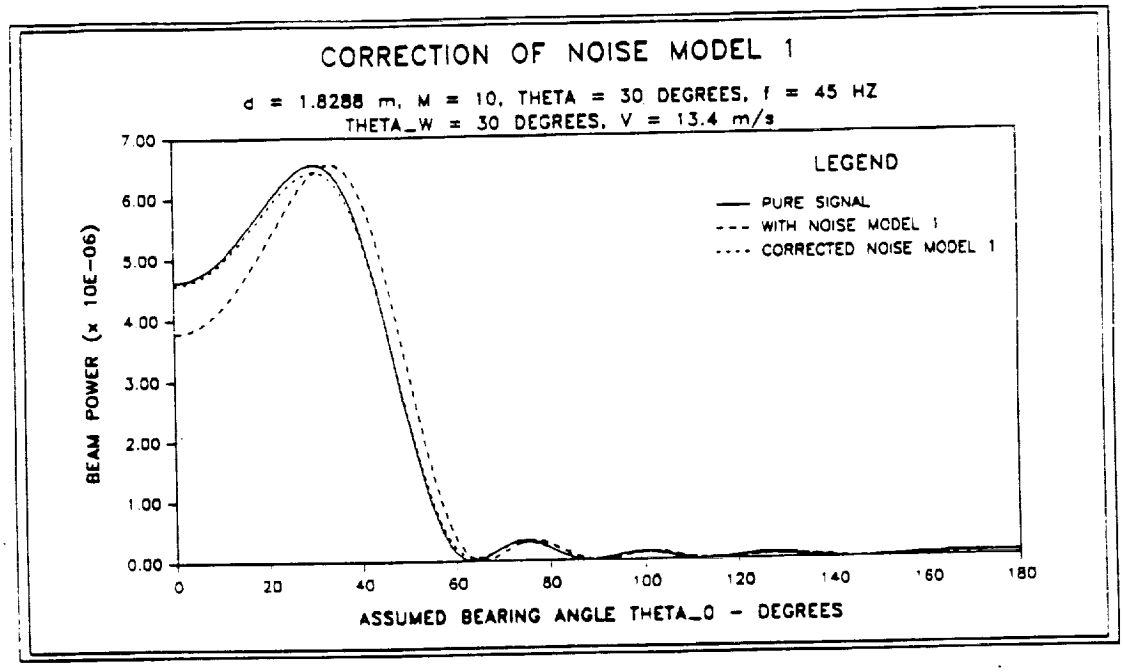

Figure 23. - Bartlett Estimate beamformer output comparing pure signal case with output including atmospheric effects modeled by Noise Model 1 and the case of the corrected Noise Model 1 for $f = 45$ Hz and $\theta = 30°$.

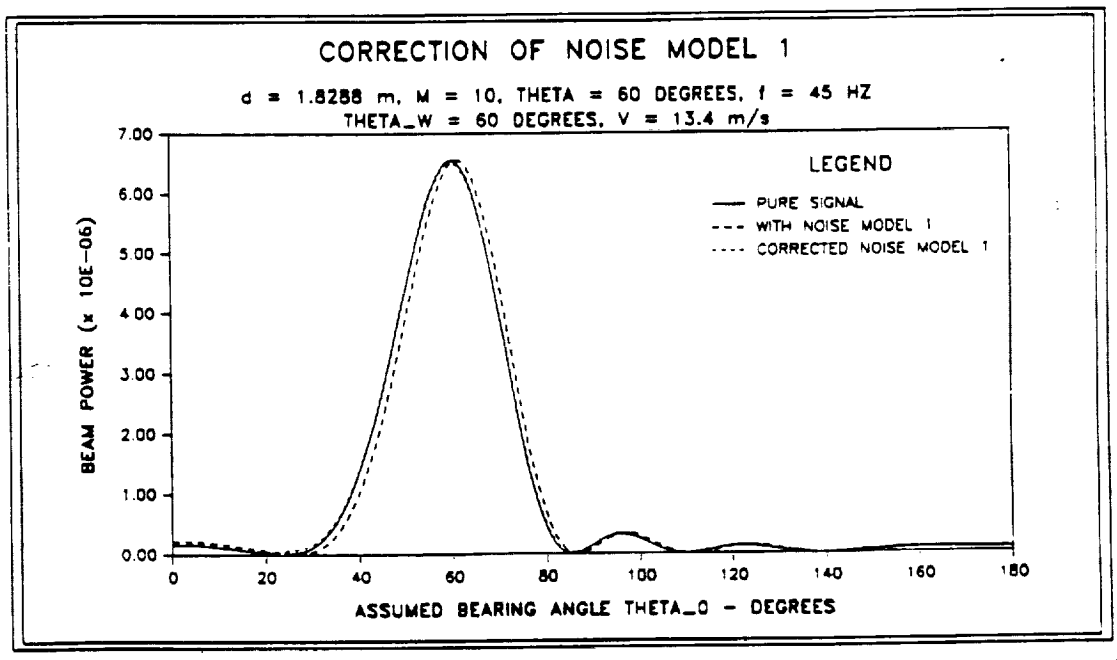

Figure 24. - Bartlett Estimate beamformer output comparing pure signal case with output including atmospheric effects modeled by Noise Model 1 and the case of the corrected Noise Model 1 for $f = 45$ Hz and $\theta = 60°$.

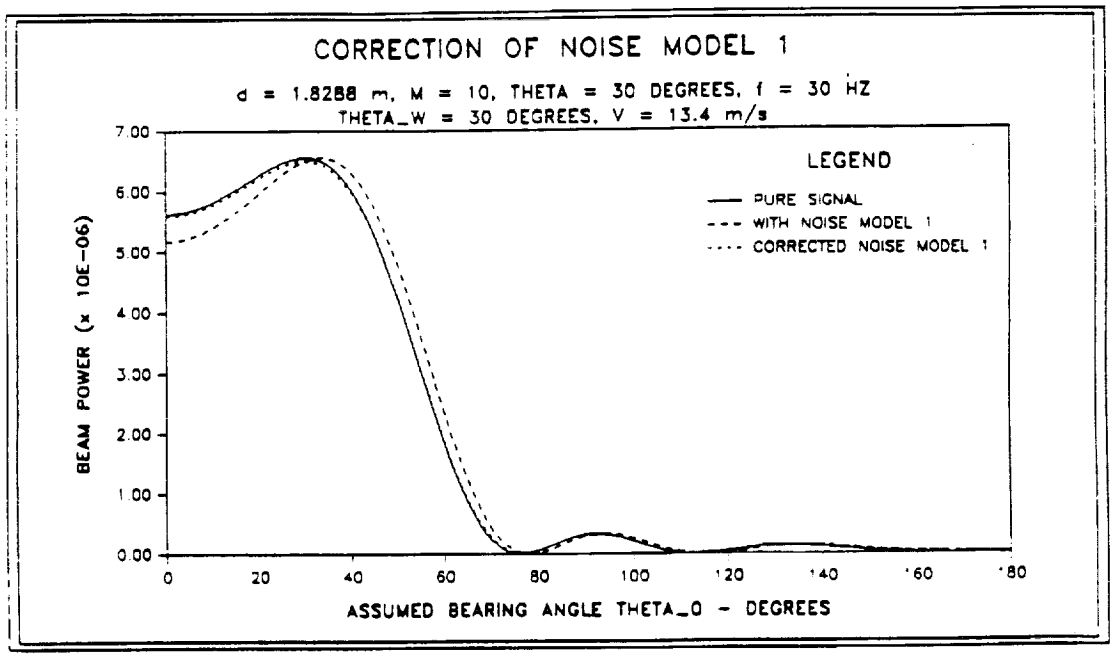

Figure 25. - Bartlett Estimate beamformer output comparing pure signal case with output including atmospheric effects modeled by Noise Model 1 and the case of the corrected Noise Model 1 for $f = 30$ Hz and $\theta = 30°$.

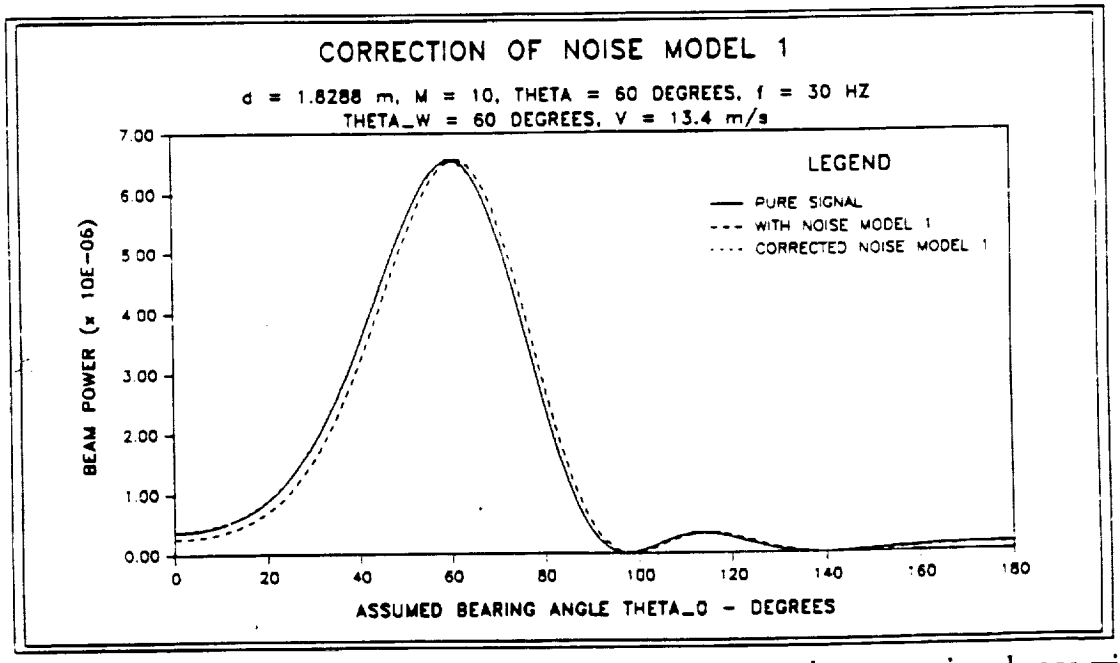

Figure 26. - Bartlett Estimate beamformer output comparing pure signal case with output including atmospheric effects modeled by Noise Model 1 and the case of the corrected Noise Model 1 for $f = 30$ Hz and $\theta = 60°$.

A unit vector in this direction is $\hat{u}_2$ with bearing angle θ_2 given by

$$\theta_2 = \tan^{-1}\left(\frac{U_{2y}}{U_{2x}}\right) + \pi \tag{4.17}$$

The propagation speed is also changed. The new propagation speed is c_2 and is given by

$$c_2 = \sqrt{U_{2x}^2 + U_{2y}^2} \tag{4.18}$$

The maximum error caused by this model occurs when $\hat{u}$ and $\hat{p}$ are orthogonal regardless of the value of θ.

This bearing angle is then used to calculate the adjusted spatial correlation matrix $\bar{R}_2$ for the noise represented by the second model. The knth element of $\bar{R}_2$ is

$$\bar{R}_{2,kn} = S(f)S^*(f)\exp\{j2\pi f\frac{(\bar{r}_k - \bar{r}_n)\cdot\hat{u}_2}{c_2}\} \tag{4.19}$$

The beam power for this beamformer simulation is

$$P(f,\hat{u}_0) = \bar{w}^+\bar{R}_2\bar{w} \tag{4.20}$$

Figures 27 through 32 give examples of output from the simulation of this noise model for frequencies of 30, 45 and 90 Hz and values of θ of 30° and 60°. The mean wind velocity V was 13.4 m/s (44 ft/sec). In each case, θ_W was set to $\theta + 90°$ to obtain orthogonality of the wind and propagation vectors.

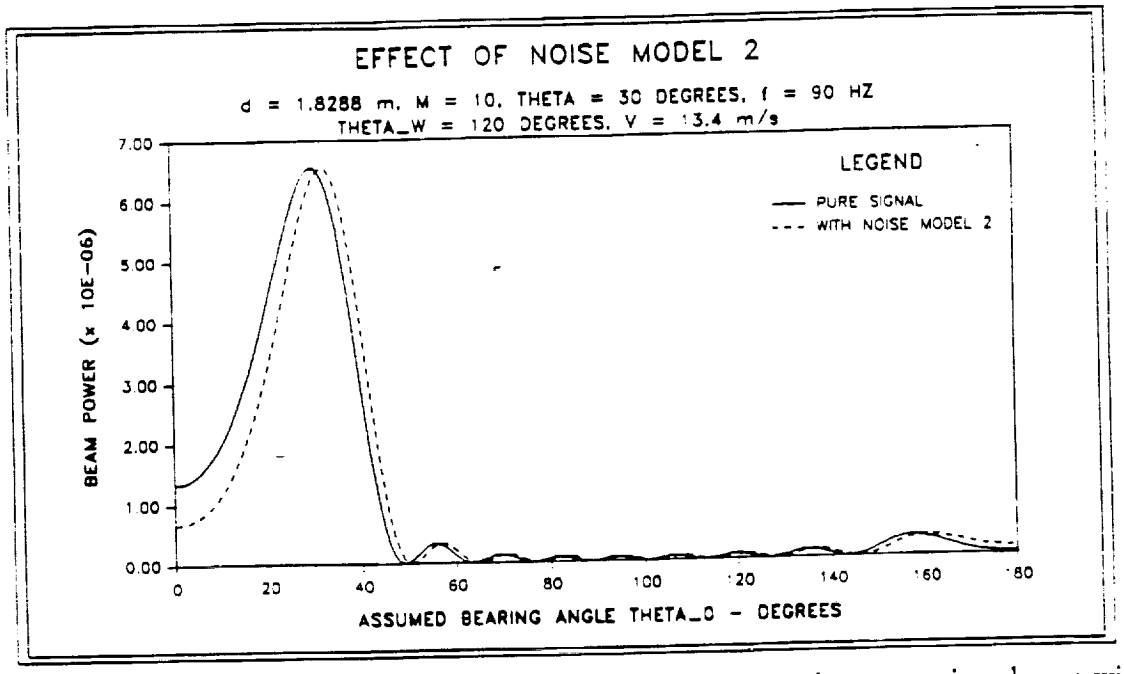

Figure 27. - Bartlett Estimate beamformer output comparing pure signal case with output including atmospheric effects modeled by Noise Model 2 for $f = 90$ Hz and $\theta = 30°$.

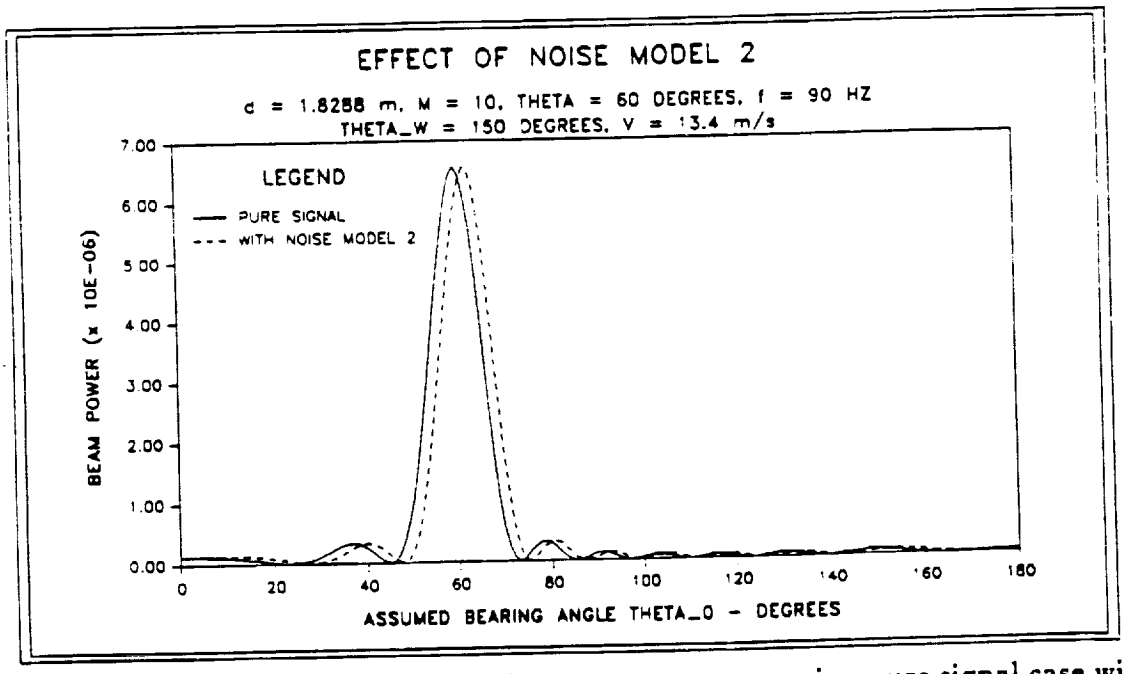

Figure 28. - Bartlett Estimate beamformer output comparing pure signal case with output including atmospheric effects modeled by Noise Model 2 for $f = 90$ Hz and $\theta = 60°$.

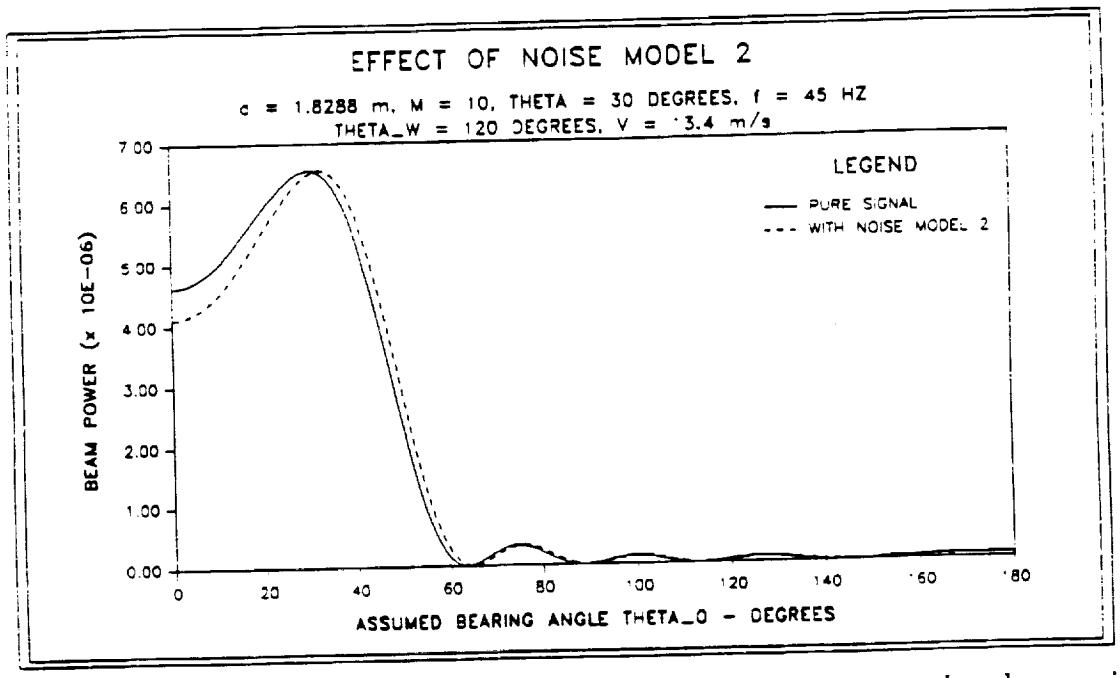

Figure 29. - Bartlett Estimate beamformer output comparing pure signal case with output including atmospheric effects modeled by Noise Model 2 for $f = 45$ Hz and $\theta = 30°$.

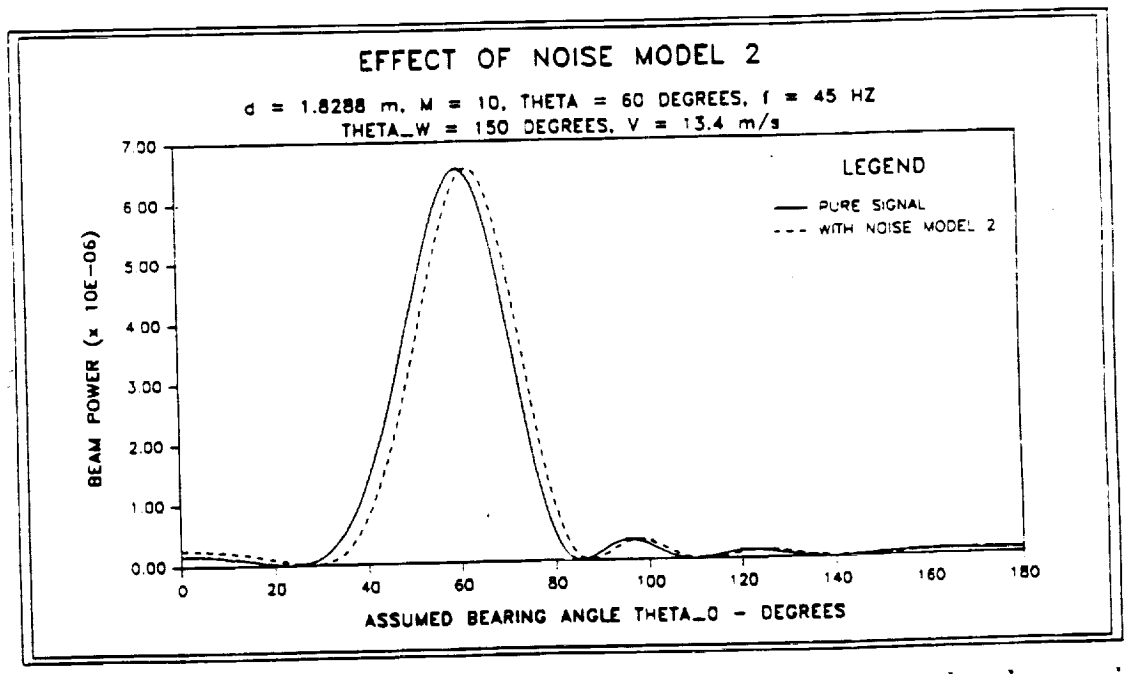

Figure 30. - Bartlett Estimate beamformer output comparing pure signal case with output including atmospheric effects modeled by Noise Model 2 for $f = 45$ Hz and $\theta = 60°$.

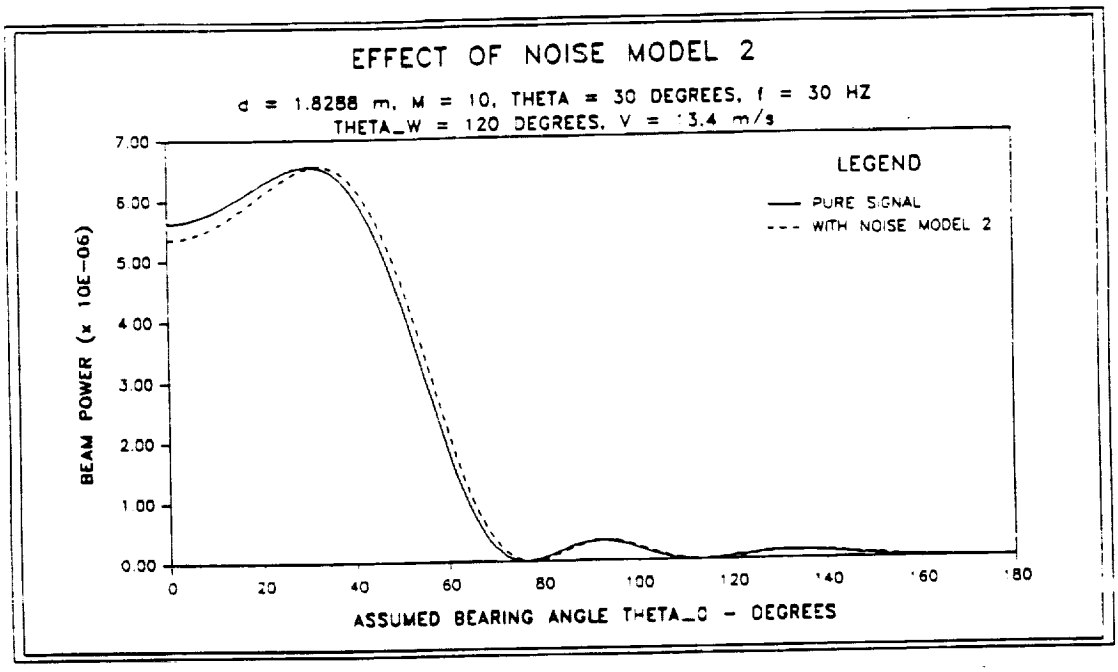

Figure 31. - Bartlett Estimate beamformer output comparing pure signal case with output including atmospheric effects modeled by Noise Model 2 for $f = 30$ Hz and $\theta = 30°$.

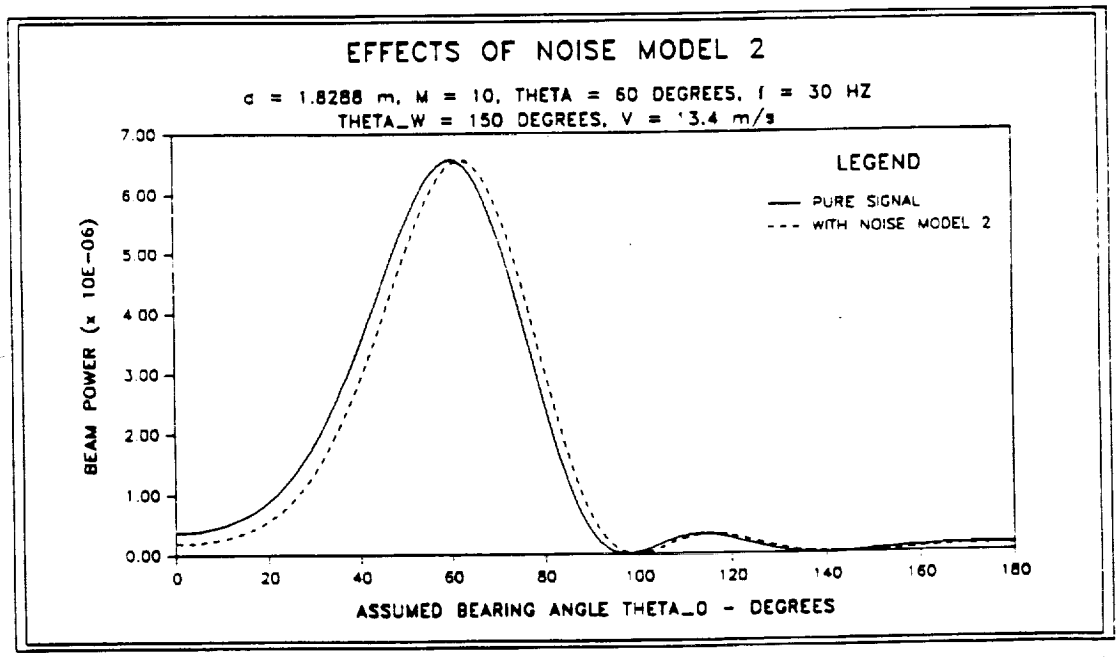

Figure 32. - Bartlett Estimate beamformer output comparing pure signal case with output including atmospheric effects modeled by Noise Model 2 for $f = 30$ Hz and $\theta = 60°$.

The first noise model was essentially a phase shift implemented by the multiplication of a complex exponential. Thus the error it induced was easily corrected. The implementation of the second noise model is more mathematically complex. The error caused by noise of this form is located in the bearing angle θ_2 locating the unit vector $-\hat{u}_2$. In calculation of the beamformer, this angle is the argument of a cosine term. The cosine term itself is in the argument of a complex exponential. Since a linear array of equally spaced sensors is the subject of this analysis, the dot product in the exponential of Equation 4.19 can be written as

$$(\bar{r}_k - \bar{r}_n) \cdot \hat{u}_2 = (k - n) d \cos\theta_2 \tag{4.21}$$

θ_2 is calculated from Equations 4.15 through 4.17. It is impossible to mathematically isolate θ_2 in order to correct for it.

Efforts made to equate the effect of this representation of noise to an effective phase shift were unsuccessful. If this were possible, the same approach to correction as taken with the first model might yield favorable correction results. Another approach considered to correct for this error was the alteration of the steering vectors w_i. Using the assumed bearing angle θ_0, it was possible to correct the beam shift at the true angle of propagation. However, this approach worsened the error in the "mirror image" of the beamformer output that exists due to the symmetry discussed in Chapter III. This symmetry must be acknowledged when using a linear array and the effects of such attempts at correcting for the error due to the wind would make the handling of the symmetry more difficult. Figure 33 presents an attempt to use the steering vectors for correction. Note that at the true propagation bearing $\theta = 45°$, the corrected output and the pure signal output are coincident. However at the symmetric location of θ_0 = -45°, the uncorrected and corrected curves are coincident. The error is not corrected at this point.

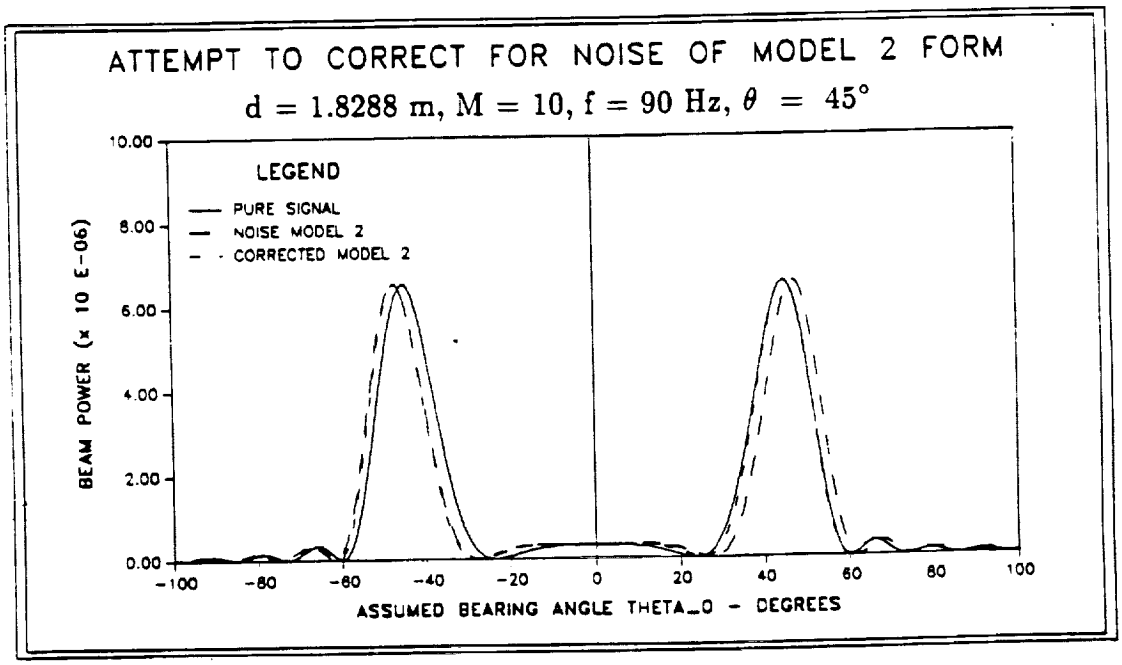

Figure 33. - Illustration of an attempt to correct the Bartlett Estimate power output for the effects caused by Noise Model 2. Modification of the steering vectors w_i was used. The true bearing angle is as 45°. The symmetry of the linear array also causes an indication at $-45°$. At $\theta_0 = 45°$, the corrected plot coincides with the plot of pure signal output. However, at $\theta_0 = -45°$, the corrected and uncorrected plots coincide. This result complicates the symmetry problem because the effect of the correction is not symmetrical about $\theta_0 = 0°$.

CHAPTER V

RESULTS, CONCLUSIONS AND RECOMMENDATIONS

A. Results of Application of Noise Models to Bartlett Estimate Beamformer

Figure 34 shows the behavior of the half power point beam width for the cases of pure signal, Noise Model 1, corrected Noise Model 1, and Noise Model 2. This figure shows that Noise Model 1 and Noise Model 2 yield a smaller beamwidth than the pure signal case and the corrected Model 1 case. For the set of parameters used in Figure 34, the data points for the beamwidth for the pure signal case and the corrected Noise Model 1 case are coincident. Also, the data points for Noise Model 1 and Noise Model 2 are coincident. The result shown is that both Noise Model 1 and Noise Model 2 have the same effect on the beam width for the same conditions at a particular frequency.

Figures 35 and 36 show the error in true bearing angle (beam shift) for Noise Model 1, corrected Noise Model 1, and Noise Model 2. The error due to Noise Model 1 is generally greater than that caused by Noise Model 2. The correction for Noise Model 1 eliminates all of the error caused by Noise Model 1 but the cost of this correction is an increased half power point bandwidth as seen in Figure 34. As all of the results show, neither of the noise models produce sidelobes. Also note that the beam shift is independent of frequency.

Both noise models cause the beam to be more narrow and they both cause some beam shift. Since Noise Model 1 has the $\cos\theta$ factor as in Equation 4.9, the error in true bearing location will depend on the value of θ as well as the

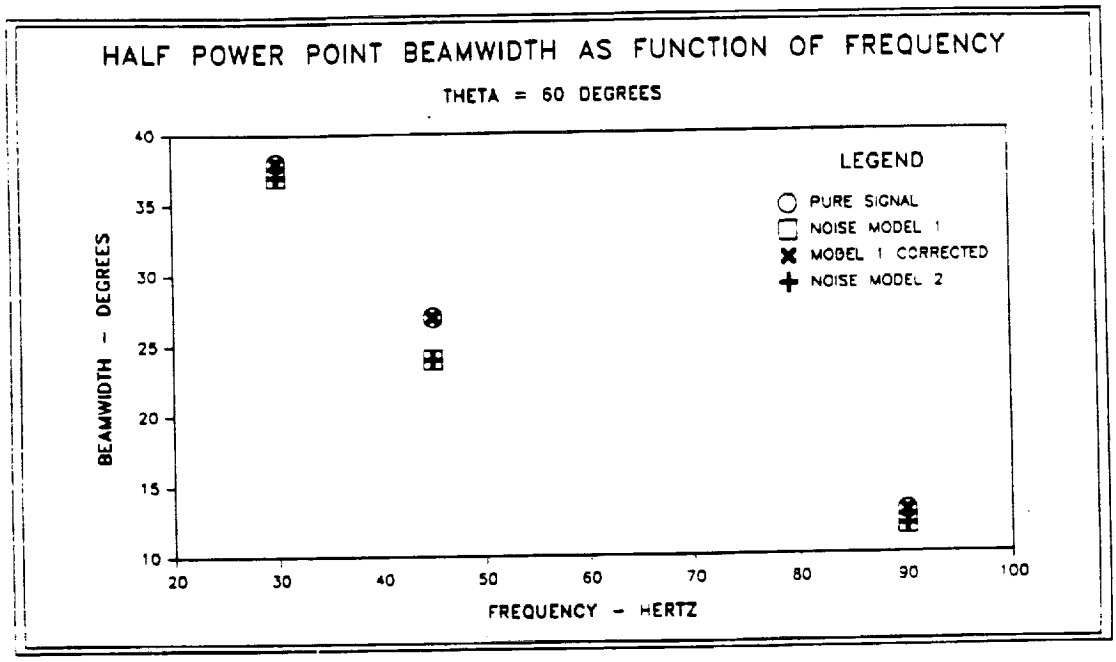

Figure 34. - Relation between the half power point beamwidth and the frequency, f. The data points for pure signal and Model 1 Corrected are coincident and the data points for Noise Model 1 and Noise Model 2 are coincident. The half power point bandwidth for the pure signal case and the corrected Model 1 case are always greater in this range of frequencies than for the cases of uncorrected Models 1 and 2 at a given frequency.

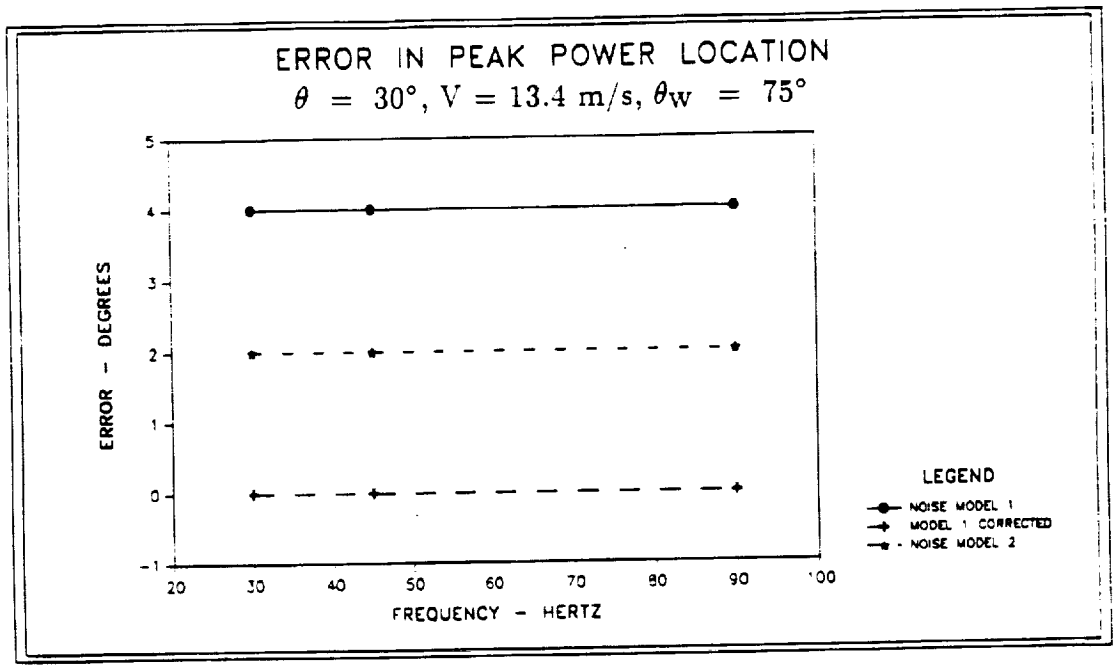

Figure 35. - Results showing the error (beam shift) in the maximum of the Bartlett Estimate beamformer output for Noise Model 1, Noise Model 2 and the correction of Noise Model 1 versus frequency for $\theta = 30°$.

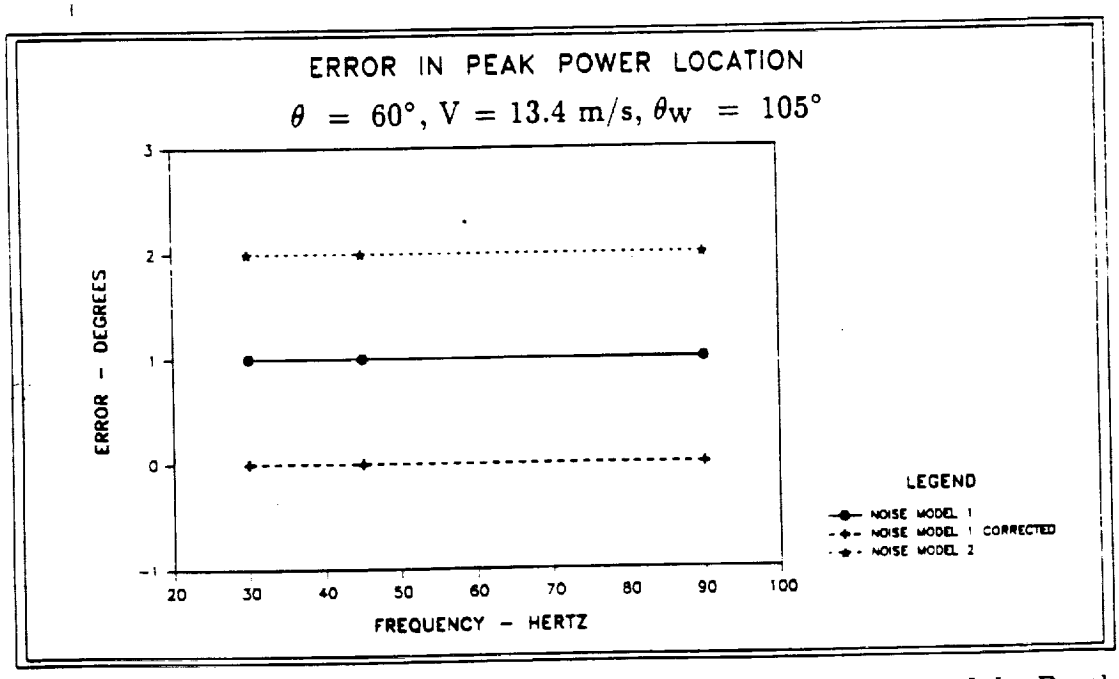

Figure 36. - Results showing the error (beam shift) in the maximum of the Bartlett Estimate beamformer output for Noise Model 1, Noise Model 2 and the correction of Noise Model 1 versus frequency for $\theta = 60°$.

wind speed and direction. Noise Model 2 only depends on the wind speed and direction. Note in Figure 36 that, for θ equal to 60°, Noise Model 2 causes more error. But, in Figure 35, Noise Model 1 causes the greater error in true bearing angle determination.

Figures 37 and 38 show the effect of wind velocity V on the magnitude of the beam shift for Noise Models 1 and 2. In each case, the values of θ, d, M, θ_W and f are constant in each of the plots. These parameter values are not the same for *both* of the plots. In each of these plots, the wind bearing angle θ_W was selected to give the greatest amount of beam shift for the value of θ used. It is clear that the error caused by each model increases with wind speed. The choice of 22.4 m/s (73.3 ft/sec) for V may seem high but it must be remembered that these are *instantaneous* velocities which may be sustained only for a fraction of a second. See Appendix B for discussion of atmospheric mean wind time scales.

Figures 39 and 40 show the effect of the true bearing angle θ on the magnitude of the beam shift over a range of θ. The values of M, d, f, V and θ_W are constant in each case (for each plot). Note that the maximum error for Noise Model 2 is seen in the middle of this range. However, for Noise Model 1, the maximum error occurs at the left end of the range for θ. This is so because the $\cos\theta$ factor in Equation 4.9 goes to zero as θ approaches $\pi/2$.

A maximum amount of beam shift for Noise Model 1 is shown in Figure 41. For a wind speed V of 13.4 m/s (44 ft/sec) and a value of θ_W selected to maximize ϕ_{kn} from Equation 4.9, beam shifts of up to 10 degrees were obtained. This is observed as θ is near 0 or 180 degrees and the quantity $(\theta_W - \theta)$ is near π. Note that as θ becomes near 30°, the magnitude of the beam shift returns to the levels shown in the previous chapter - about four degrees and less. The wind conditions in

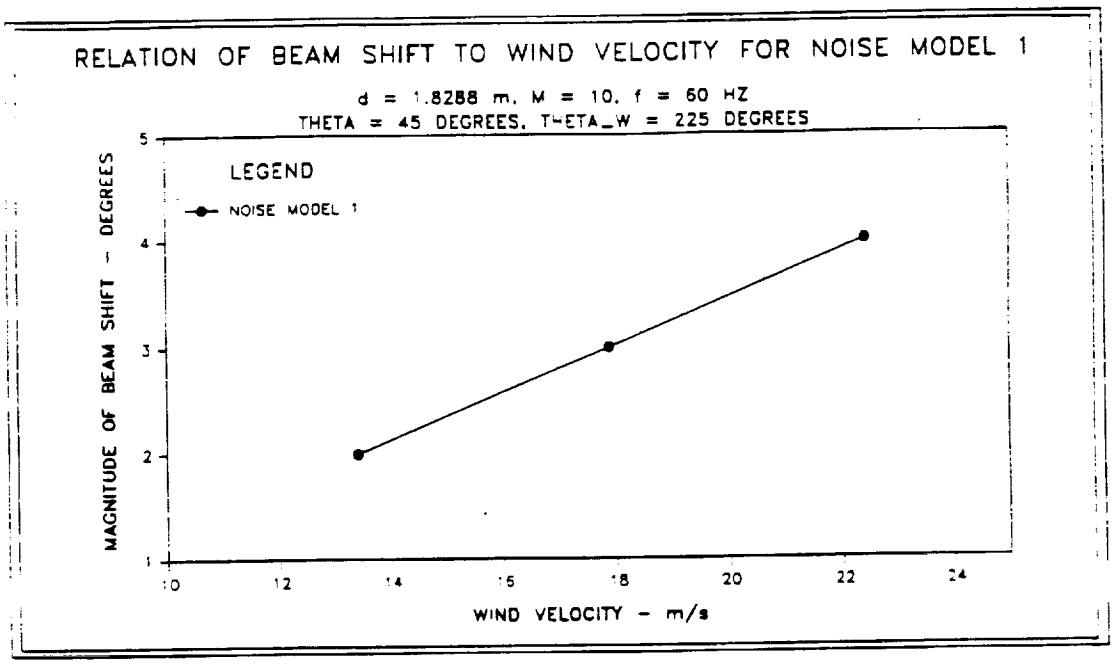

Figure 37. - Relation of beam shift to wind velocity for Noise Model 1.

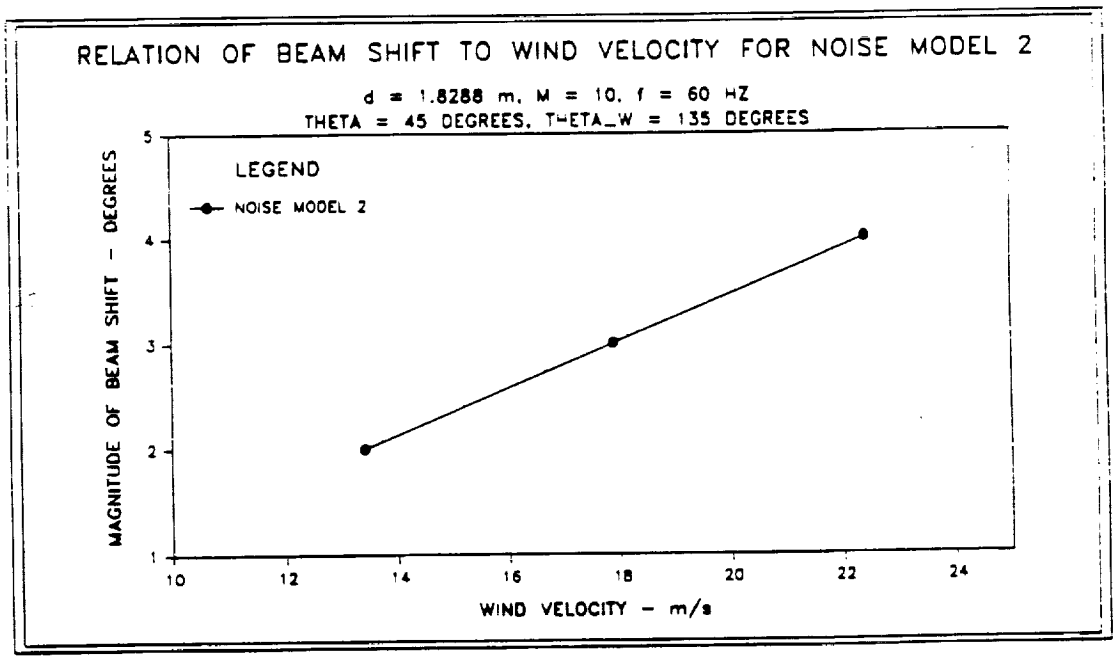

Figure 38. - Relation of beam shift to wind velocity for Noise Model 2.

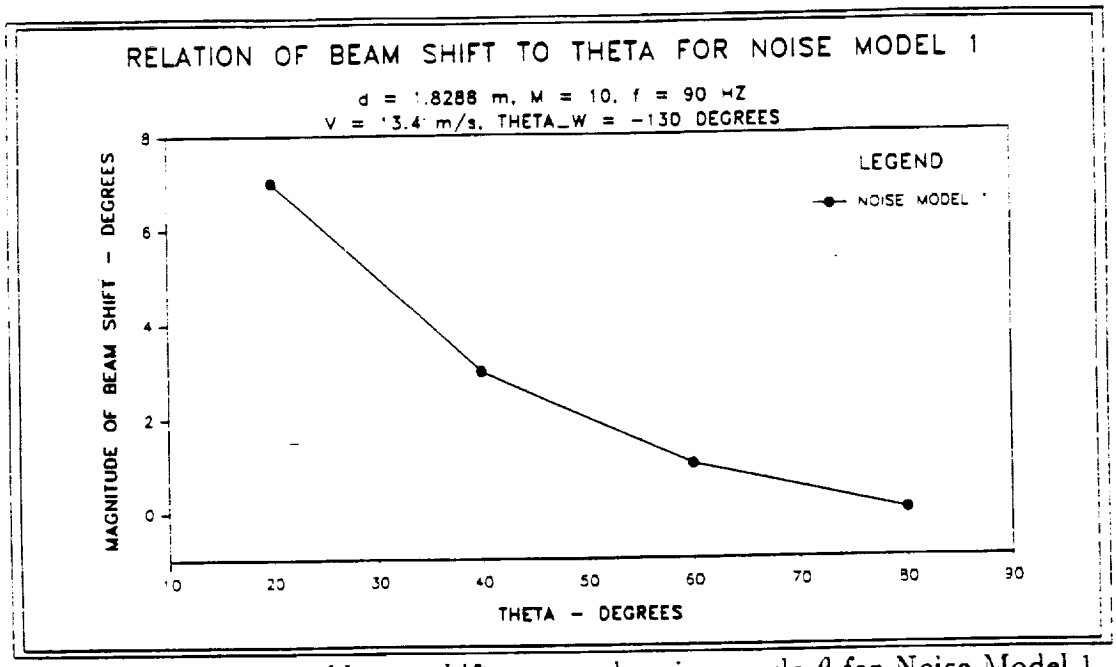

Figure 39. - Relation of beam shift to true bearing angle θ for Noise Model 1.

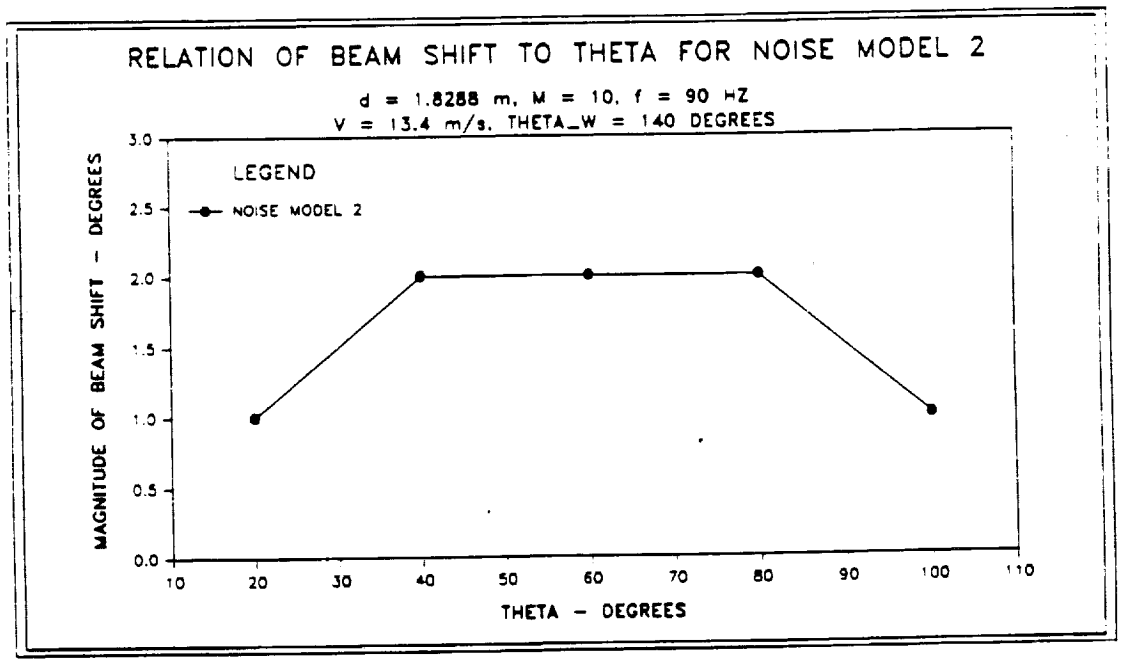

Figure 40. - Relation of beam shift to true bearing angle θ for Noise Model 2.

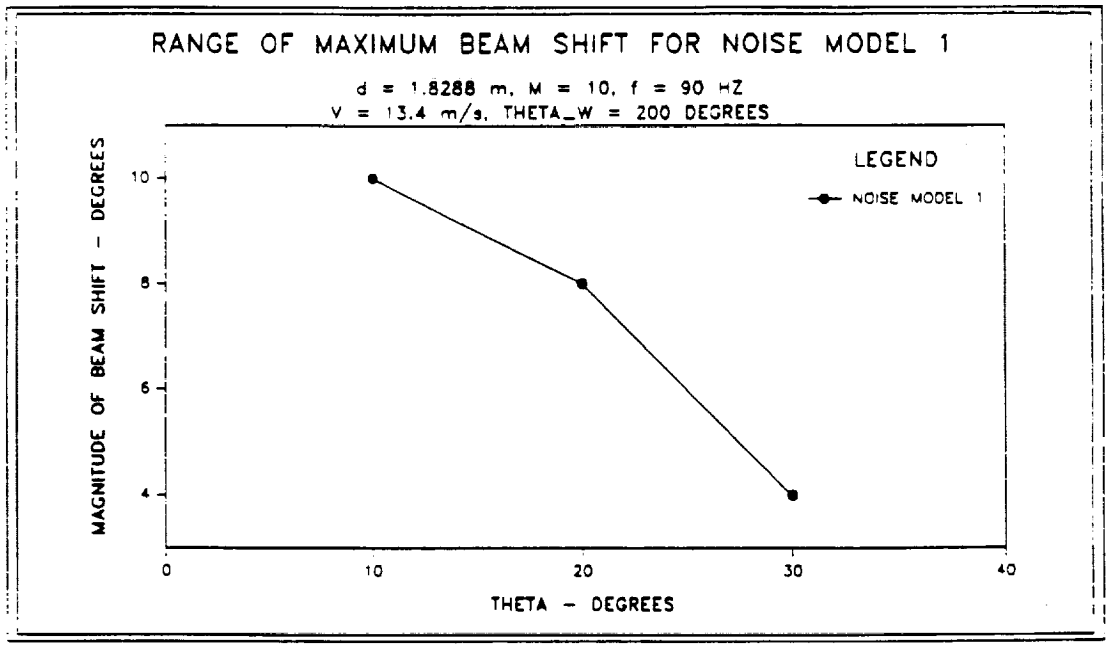

Figure 41. - Maximum beam shift observed for Noise Model 1 in the range of θ_0 near θ_0 equal to zero.

Figures 39 and 41 are not the same. As both figures show, the beam shift increases as θ approaches zero degrees. It is not shown in Figure 39, but as Figure 41 shows, as θ becomes less than about 20°, the amount of beam shift levels off and reaches a maximum magnitude of about 10 degrees. For wind speeds of up to 22.4 m/s (73.3 ft/sec), beam shifts near 0 and 180 degrees of up to 20 degrees may be seen.

B. Conclusions Regarding Validity of Current Work

Wind in the atmosphere degrades the performance of the Bartlett Estimate beamformer when used for tracking applications where the time for data sampling and processing is relatively short. This report has addressed one case of instantaneous atmospheric conditions. This case is a wind of constant velocity blowing over an array of sensors in one direction.

Two models were proposed to mathematically represent the effect of mean wind on the Bartlett Estimate beamformer. Simulations were run and the effects were quantified.

In the case of Noise Model 1, it was possible to correct, in closed form, for the effect of the mean wind. This model is the more idealized one. If in fact the mean wind may be represented by Model 1, the effect of the wind may be eliminated in the Bartlett Estimate algorithm. This was demonstrated in Chapter IV.

For Noise Model 2, no closed form solution is available. The mathematics of the second model are more complex and an algebraic or trigonometric isolation of the error in bearing angle is not possible. More work is necessary to determine if perhaps an empirical correction for Noise Model 2 is possible.

In the case of both of the noise models presented here however, the effects of the wind models are not as pronounced as expected. No obvious sidelobes were produced and no widening of the half power point beam width was caused. The only error caused by these models was a shift in the location of the maximum in the beam power which indicates the true bearing angle. The beam shift was generally four degrees and less. However, as was shown in Figure 41, beam shifts of 10 degrees are possible with Noise Model 1. It has been proposed that these beamforming techniques could be used to track targets 24.1 km (15 mi) away. A four degree error in bearing equates to approximately a 1.69 km (1.05 mi) error in location at a range of 24.1 km (15 mi). A beam shift of 10 degrees caused a 4.21 km (2.6 mi) error in location of the source. Therefore, this error could be appreciable depending on the conditions and the application.

The work done in this report has three important results.

1) These models do cause one effect seen in actual results. This effect is the beam shift. Previously proposed models do not explain *any* of the three detrimental effects on the Bartlett Estimate beamformer. Thus, the present work is an improvement over prior work in this subject area in that at least one cause of beam shift has been identified.

2) If the mean wind blowing over the array may be represented by the models derived and presented here, its effects have been quantified. And in the case of the first model, the effects of the mean wind may be corrected. If the amount of beam shift observed is deemed insignificant for the application, then effects of mean wind may be ignored and would be assumed to not effect the Bartlett Estimate in any crucial way.

3) Since these models do not cause any sidelobes or increase in the half power point beamwidth as seen in actual experimental results, it must be concluded that the mean wind *does not cause these effects.* These effects must be caused by some other conditions in the atmosphere. There are many other instantaneous wind conditions which have not been addressed here.

Some recommendations for continued work in this area are now made.

C. Recommendations

1) Conduct experimental verification studies in a controlled environment. The experiments would demonstrate the correctness of the two models presented here; experiments would also identify what atmospheric parameters need to be measured in addition to the sound.

2) Further literature search/experimental work is required to quantify the instantaneous wind speed and direction descriptors in the lower atmosphere. Address how to ascertain reasonable parameters for a wind gust and how to properly model turbulent eddies over a sensor array.

3) Perform additional analytical studies (simulations) to determine the effects of array geometry, frequency, sensor spacing and the number of sensors deployed.

REFERENCES

Burdic, William S., 1984, *Underwater Acoustic Systems Analysis*, Prentice-Hall, Englewood Cliffs, NJ.

Capon, J., 1969, "High-resolution frequency-wavenumber spectrum analysis," *Proc. IEEE,* Vol. 57, No. 8, pp. 1408-1418.

Daigle, G. A., J. E. Piercy, and T. F. W. Embleton, 1978, "Effects of atmospheric turbulence on the interference of sound waves near a hard boundary," *J. Acoust. Soc. Am.,* Vol. 64, No. 2, August, pp. 622-630.

Daigle, G. A., T. F. W. Embleton, 1986, "Propagation of sound in the presence of gradients and turbulence near the ground," *J. Acoust. Soc. Am.,* Vol. 79, No. 3, March, pp. 613-627.

Gerhold, Carl H., 1990, private communication.

Johnson, Don H., 1982, "The application of spectral estimation methods to bearing estimation problems," *Proc. IEEE,* Vol. 70, No. 9, September, pp. 1018-1028.

Kleyn, A. H., 1983, *Seismic Reflection Interpretation*, Applied Science Publishers Ltd., New York, NY.

Nielsen, Richard O., 1989, "Acoustic Signal Processing," Seminar, Orlando, Florida, Sponsored by Technology Training Corporation, February 8-10.

North, Gerald R., (1990), private communication.

Piercy, J. E., T. F. W. Embleton and L. C. Sutherland, 1977, "Review of propagation in the atmosphere," *J. Acoust. Soc. Am.,* Vol. 61, No. 6, June, pp. 1403-1418.

Strum, Robert D. and Donald E. Kirk, 1988, *First Principles of Discrete Systems and Digital Signal Processing,* Addison-Wesley, Reading, MA.

Stull, Roland B., 1988, *An Introduction to Boundary Layer Meteorology*, Kluwer Academic Publishers, Dordrecht, The Netherlands.

APPENDIX A

DIGITAL SIGNAL PROCESSING CONSIDERATIONS

The subject matter of this report is not concentrated on the practical implementation of beamforming. However, two points should be mentioned. The relative magnitude of the beam power calculated is dependent on the number of FFT points, N, taken in the data sampling. As the length of the sampled input sequence is increased, more summations are carried out in the Fast Fourier Transform algorithm. This increases the magnitudes of the Fourier terms $S(f)$ in Equation 2.7.

The choice of digital sampling frequency, f_s, and N determine the frequency resolution of the beamformer. The frequency resolution is the "spacing" between frequency components and is given by

$$\Delta f = \frac{f_s}{N} \tag{A.1}$$

If the sampled sensor output has frequency components that are closer together than Δf, these components will not be represented as separate and distinct frequencies. Instead, "smearing" will result and the contribution to the spectrum from the in-between frequency components will be distributed among adjacent frequency components as discussed by Strum and Kirk (1988). The magnitudes of the Fourier Transforms of these components $S(f)$ will be less than if the frequency component of the sampled data did not fall between Fourier components. When the beamformer calculates beam power for frequencies in a range where smearing has occurred, the magnitude of the beam will be somewhat less than those for frequency components which match exactly with frequencies in the sampled input sequence. Some digital signal processing techniques must be applied to maintain the performance of the beamformer. These techniques fall into the area of discrete spectrum analysis and

are beyond the scope of this report. A knowledge of the *acoustic signature* of the target is helpful. Selecting N and f_s such that a fine frequency resolution is obtained over the range of interest aids in keeping a uniform beam power output. The sampling frequency, f_s, must also be chosen such that *frequency* aliasing is avoided. f_s must be at least twice the highest frequency in the sampled signal to avoid frequency aliasing.

These issues were not addressed in the simulation done in this report. A value of unity for Δf was used in all cases and all frequencies tested were integer values. These considerations are critical in practical application of the Discrete Fourier Transform to beamforming.

APPENDIX B

ATMOSPHERIC MEAN WIND TIME SCALE

Scales of time, length and velocity are commonly used in meteorology to quantify a time, length or velocity characteristic to a particular situation. A time scale is the length of time it generally takes for a certain action to occur as discussed by Stull (1988). There are many derived meteorological time scales. Some are for the stratification of the atmosphere. These time scales may be on the order of hours. Other time scales are for the viscous dissipation of energy by eddies on the order of one millimeter in size. Time scales such as these may be on the order of a fraction of a second. In this report, atmosheric phenomena are addressed which have time scales on the order of one second. The effect of mean wind on the performance of the Bartlett Estimate is the subject of this thesis. The motion of a large air mass is what causes the mean wind effects. According to Stull (1988), the time scale for such an action is $x/\bar{U}$ where x is the distance travelled and $\bar{U}$ is the mean velocity of the air mass. Depending on the relative magnitudes of these values, this time scale may be on the order of one second to one minute. For the cases shown in this report, x, the length of the array, is 16.5 m (54 ft) and $\bar{U}$ is 13.4 m/s (44 ft/sec). The time scale for this sensor arrangement is approximately 1.25 seconds. It is assumed then that the wind conditions will remain constant over the array for 1.25 seconds. This is greater than the 0.5 second sampling time over which data is recorded. Therefore, the average of the data taken over the 0.5 second time window is assumed to be representative of the instantaneous atmospheric conditions at that time.

For the case of a 22.4 m/s (73.3 ft/sec) wind as mentioned in Chapter V, this assumption still holds true. The mean wind time scale for the same array with a wind speed of 22.4 m/s (73.3 ft/sec) is about 0.75 second. While this length of

time is not an order of magnitude greater than the 0.5 second sampling time, it still considered to be of sufficient length over which to obtain representative average data.

These assumptions are required for the Bartlett Estimate to be simulated as it was in this report. Atmospheric conditions are so unpredictable that such assumptions are necessary in almost any such study. The model presented in Chapter III that assumed the noise to be spatially white and homogeneous is an example of this necessity. In water, where that model is most often used, objects move much slower and longer sampling ang averaging times can be had. In the atmosphere, this is not the case. Therefore, these assumptions must be made to apply the technology which is already known to new and different conditions.

APPENDIX C

THREE MODELS FOR THE SPATIAL CORRELATION OF NOISE

This appendix presents three models that were obtained from Burdic (1984) and essentially have been applied to three dimensional use in the ocean. The derivations of these models are not provided here and may be obtained in Burdic's text. See Figure 42 for illustrations of these models.

1) Isotropic Noise - The isotropic noise model assumes that acoustic energy due to noise is distributed evenly over a sphere and uniformly over all frequencies and bearing angles. The ijth element of $\bar{Q}$ for isotropic noise is given by

$$q_{ij}(d_{ij}, \lambda, \tau) = \frac{\sin(4\pi d_{ij}/\lambda)}{(4\pi d_{ij}/\lambda)} \tag{C.1}$$

d_{ij} is the distance between the sensors, λ is the wavelength corresponding to frequency f, and τ is the time delay incurred over the distance traveled ($\tau = d_{ij}/c$). These definitions also hold for the next two models presented.

2) Semi-Isotropic Noise - The semi-isotropic noise model assumes that the acoustic energy due to noise is uniformly distributed over a symmetric portion of a sphere cut by an angle ϕ_0. The ijth element of $\bar{Q}$ for this model is given as

$$q_{ij}(d_{ij}, \lambda, \tau) = \text{sinc}\{2d_{ij}\cos(\phi_0)/\lambda\}\cos(2\pi c\tau/\lambda) \tag{C.2}$$

For an array on the ground, a value of zero degrees is used for ϕ_0. The sinc function is defined such that $\text{sinc}(x) = [\sin(x)]/x$.

3) Impulsive Noise - The noise is considered uniformly isotropic over a region everywhere in azimuth at an angle of elevation ϕ_0 and zero elsewhere. The ijth element of the matrix $\bar{Q}$ is given by

$$q_{ij}(d_{ij}, \lambda) = \text{J}_0[(2\pi d_{ij}\cos(\phi_0))/\lambda] \tag{C.3}$$

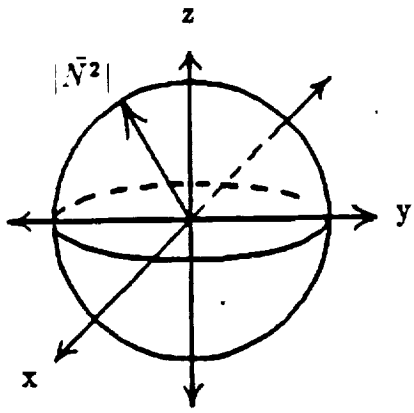

(a) Isotropic $|\bar{N}^2| = \sigma_n^2$

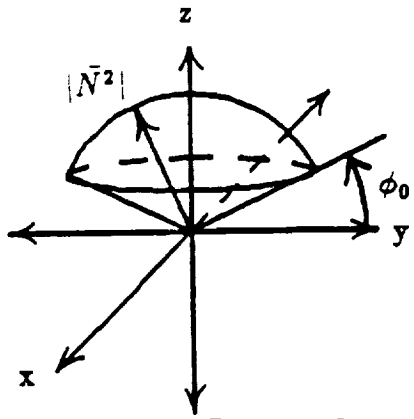

(b) Semi – Isotropic $|\bar{N}^2| = \sigma_n^2$ for $\phi \geq \phi_0$

$= 0$ otherwise

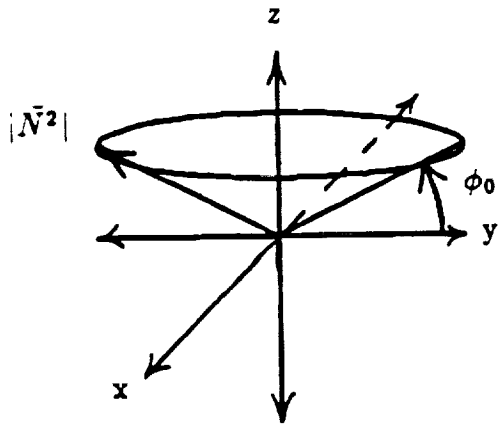

(c) Impulsive $|\bar{N}^2| = \sigma_n^2 \delta(\phi - \phi_0)$

Figure 42. - Three noise models obtained from Burdic (1984).

$J_0(\bullet)$ denotes a first order Bessel function of the first kind. A value of zero degrees is used for ϕ_0 for an array on the ground.

For each of these three models, a simulation was run to examine the results when applied to the Bartlett Estimate beamformer of Equation 2.13. The simulations were done with a linear array of equally spaced sensors at a frequency of 90 Hz with $M = 10$, $d = 1.8288$ m (6 ft), $SNR = 1$, and a true bearing angle θ of 45°. The results of these simulations compared with beamformer output containing only pure signal are given in Figures 43 through 45.

In each case, there are no sidelobes present to indicate false sources. There are only extraneous levels of power output at assumed bearing angles other than θ. There is also no error in the indication of the correct bearing angle θ. Figure 43 shows noise modeled as being isotropic as in Case 1 above. Here again the extraneous output is about 17 dB below the maximum value of beam power. Figure 44 shows the noise modeled as being semi-isotropic as described in Case 2 above. This model yields the greatest level of extraneous power output at 11 dB below the peak value. Figure 45 shows noise modeled as impulsive as in Case 3 above. There is a 13 dB difference between the main peak and the extraneous power output caused by this model. The magnitude of the beamformer power output away from the true bearing angle θ is not great enough to be considered detrimental to the beamformer performance. The absence of sidelobes indicate that these models do not cause the noise effects characteristic to actual beamforming results. Also, the half power point beam width of the main peak is not affected. Thus, these three models are inappropriate for tracking purposes.

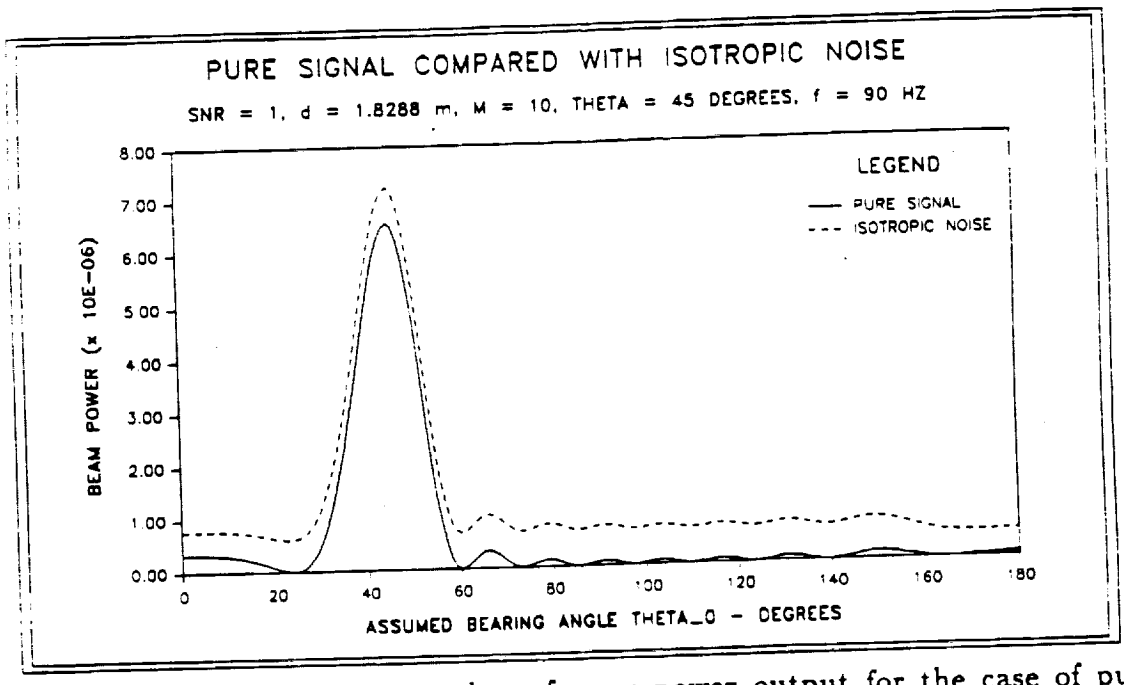

Figure 43. - Bartlett Estimate beamformer power output for the case of pure signal compared with case including noise modeled as being isotropic as described by Burdic (1984).

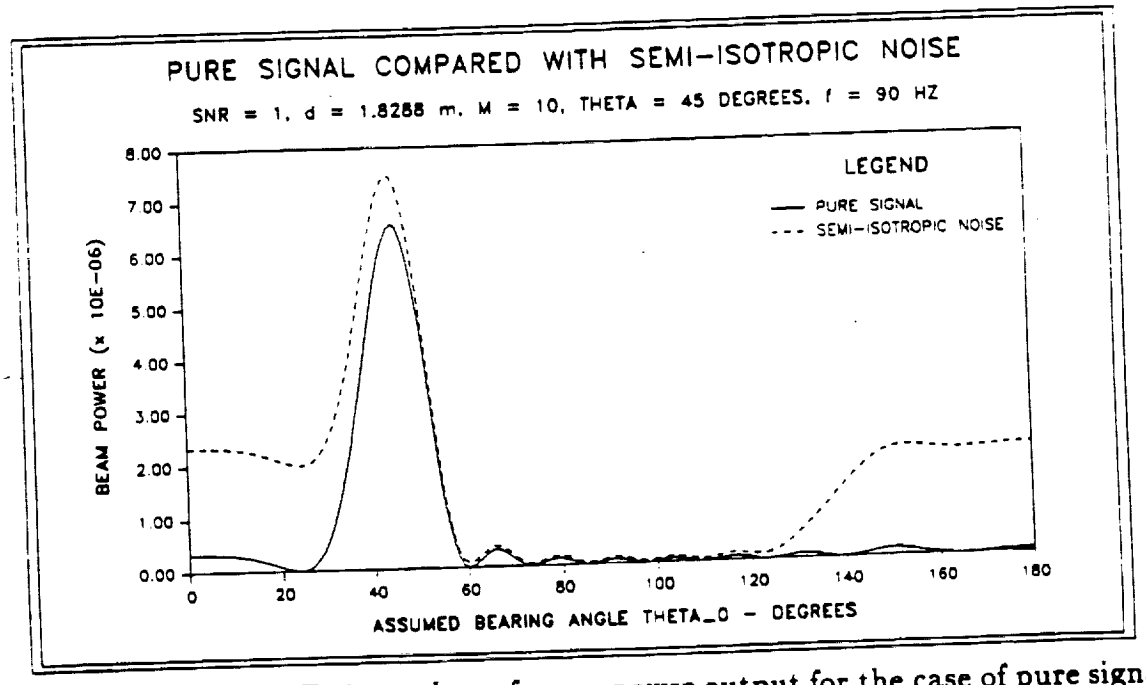

Figure 44. - Bartlett Estimate beamformer power output for the case of pure signal compared with case including noise modeled as being semi-isotropic as described by Burdic (1984).

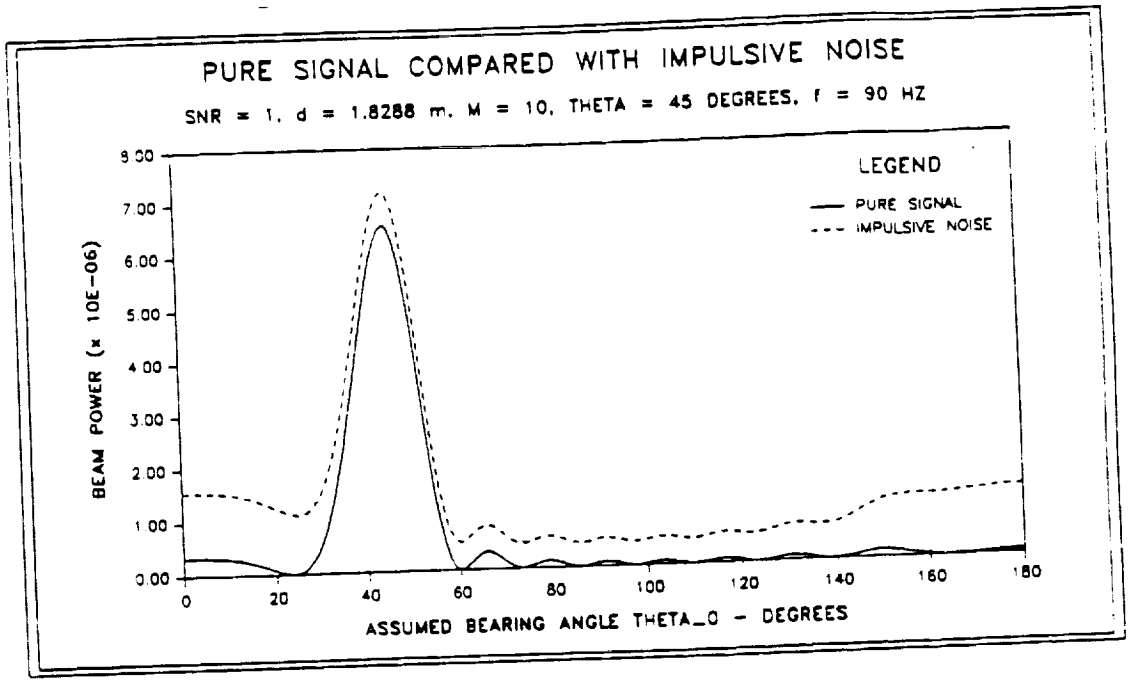

Figure 45. - Bartlett Estimate beamformer power output for the case of pure signal compared with case including noise modeled as being impulsive as described by Burdic (1984).